

# 1 Basic chemical compositions combination rules and quantitative criterion of red beds

2

3 Guangjun Cui <sup>1,2</sup>, Jin Liao <sup>2</sup>, Linghua Kong <sup>2</sup>, Cuiying Zhou <sup>2,\*</sup>, Zhen Liu <sup>2,\*</sup>, Lei Yu <sup>2</sup>, Lihai Zhang <sup>3</sup>

4

5 <sup>1</sup> Institute of Estuarine and Coastal Research/Guangdong Provincial Engineering Research Center of  
6 Coasts, Islands and Reefs, School of Ocean Engineering and Technology, Sun Yat-sen University,  
7 Guangzhou 510275, China

8 <sup>2</sup> Guangdong Engineering Research Center for Major Infrastructures Safety, Sun Yat-sen University,  
9 Guangzhou, 510275, China

10 <sup>3</sup> The University of Melbourne, Melbourne VIC 3010, Australia

11 \*Correspondences: [zhoucy@mail.sysu.edu.cn](mailto:zhoucy@mail.sysu.edu.cn) (C. Zhou), [liuzh8@mail.sysu.edu.cn](mailto:liuzh8@mail.sysu.edu.cn) (Z. Liu)

12

## 13 Abstract

14 Red beds belong to slippery formations, and their rapid identification is of great significance for  
15 major scientific and engineering issues such as geological hazard risk assessment and rapid response.  
16 Existing research often identifies red beds from a qualitative or semi quantitative perspective, resulting  
17 in slow recognition speed and inaccurate recognition results, making it difficult to quickly handle  
18 landslide geological disasters. Combined with the correlation between red beds geomorphic  
19 characteristics, mineral compositions, and chemical compositions, this study established a preliminary  
20 identification quantitative criterion based on the basic chemical composition combination rules  
21 ( $\text{SiO}_2+\text{Al}_2\text{O}_3$ ,  $\text{Al}_2\text{O}_3/\text{SiO}_2$ ,  $\text{FeO}+\text{Fe}_2\text{O}_3$ ,  $\text{Fe}_2\text{O}_3/\text{FeO}$ ,  $\text{K}_2\text{O}+\text{Na}_2\text{O}$ ,  $\text{Na}_2\text{O}/\text{K}_2\text{O}$ ,  $\text{CaO}+\text{MgO}$ , and  $\text{MgO}/\text{CaO}$ )  
22 in the red beds. Then, perform principal component analysis on the basic chemical composition  
23 combination rules mentioned above. The results indicate that simultaneously meeting the following  
24 principal component features can serve as a rapid quantitative criterion for distinguishing red beds from  
25 other rocks:  $F1=-3.36\sim 23.55$ ,  $F2=-23.00\sim 3.11$ ,  $F3=-10.12\sim 4.88$ ,  $F4=-2.21\sim 4.52$ ,  $F5=-0.97\sim 7.30$ , and  
26  $F=-0.67\sim 1.89$ . By comparing the chemical composition combinations of 15 kinds of rocks collected  
27 from China in this study, it is proven that the quantitative criterion proposed in this study are effective.  
28 The study results can be used for rapid identification of red beds, achieving risk assessment and rapid

29 response of geological disasters such as landslides.

30 **Keywords:** red beds, quantitative criterion, geological disasters, rapid response, chemical compositions

31

## 32 **1. Introduction**

33 Red beds are widely distributed throughout the world (Zhou et al., 2023b; Yan et al., 2019; Chen  
34 et al., 2021). Geological disasters occur frequently in the red beds distribution area, especially landslides,  
35 debris flows, collapses, and underground engineering damage (Chen et al., 2014; Zhou et al., 2023a;  
36 Wang et al., 2022b). According to the characteristics of disasters such as landslides, the red beds belong  
37 to “landslide prone strata”, and the instability of slopes with weak interlayers of the red beds is  
38 particularly evident (Zhang et al., 2015). This is mainly due to the strong hydrophilicity and weak  
39 permeability of the red beds, which are prone to softening and plastic deformation under the action of  
40 water; After absorbing water, the red beds are easy to expand, and after losing water, they are easy to  
41 contract; The weathering resistance of the red beds are weak, they are easy to collapse, and their  
42 compressive and shear strength are low (Zhang et al., 2016; Wu et al., 2018; Wang et al., 2017; Marat  
43 et al., 2022; Zhang et al., 2024). The red beds have different lithology or poor binding force with other  
44 rock strata, which can easily cause differential deformation and lead to rock mass sliding along the  
45 bedding plane (Liu et al., 2020; He et al., 2023; Wang et al., 2024). Therefore, the identification of rock  
46 types, especially the rapid determination of red beds, is of great significance for major scientific and  
47 engineering issues such as risk assessment and rapid response of geological disasters in red beds  
48 distribution area.

49 At present, the studies on red beds identification are mostly carried out from the perspectives of  
50 geomorphic characteristics, mineral compositions, and chemical compositions (Cui et al., 2022; Zhou  
51 et al., 2021). And, there is a close relationship between these perspectives (Moonjun et al., 2017;  
52 Bankole et al., 2016; Perri et al., 2013). For example, the content of  $\text{Fe}_2\text{O}_3$  or hematite in the red beds  
53 is higher than that in the grey beds (Hu et al., 2006). Among these perspectives, the research of  
54 geomorphic characteristics and mineral compositions mostly adopts qualitative or semi quantitative  
55 methods, and there are many such studies. For example, Rainoldi et al. (2015) identified red beds by  
56 studying the color of geomorphic characteristics and hematite in mineral compositions, and studied the

57 mechanism of red beds bleaching. Uchida et al. (2000) distinguished red sandstone, yellowish brown  
58 sandstone, and green sandstone according to the content of hematite, goethite, biotite, and muscovite in  
59 the mineral compositions, analyzed the characteristics of different rocks and pointedly protected  
60 Angkor monuments. Xue et al. (2023) distinguished red mudstone and red sandstone by quantifying the  
61 clay mineral content in the mineral compositions, in order to analyze the mechanisms and control factors  
62 of summer uplift of high-speed railway cutting. At this stage, the research on the geomorphology,  
63 mineral color and clay content of the red beds lays the foundation for the identification of the red beds,  
64 but this identification is still vague and needs to be further quantified. Therefore, some scholars have  
65 conducted quantitative studies on the chemical compositions of red beds. Hong et al. (2009) analyzed  
66 the alteration of clay minerals by studying the changes in the  $\text{SiO}_2/\text{Al}_2\text{O}_3$  ratio in the chemical  
67 compositions of the red beds, thereby obtaining the weathering degree of the red beds. Bankole et al.  
68 (2016) studied the relationship between Fe/Mg ratio,  $\text{Fe}^{3+}/\text{FeT}$  ratio, and Cr/Fe ratio of red beds to  
69 indirectly study the oxygen content of the Paleoproterozoic. Hu et al. (2006) studied the characteristics  
70 of high  $\text{Fe}_2\text{O}_3$  content and low FeO content in the oceanic red beds, and analyzed ancient landslides on  
71 the continental margin from the perspective of petrology. However, these studies do not distinguish  
72 between red beds and other rocks in terms of chemical compositions. The use of portable spectrometers  
73 and drone-borne multi-sensor remote sensing technique can quickly obtain the chemical compositions  
74 of rocks in geological disasters while ensuring safety (Triantafyllou et al., 2021; Kirsch et al., 2018),  
75 making it feasible to use chemical compositions as the standards to distinguish red beds from other  
76 rocks.

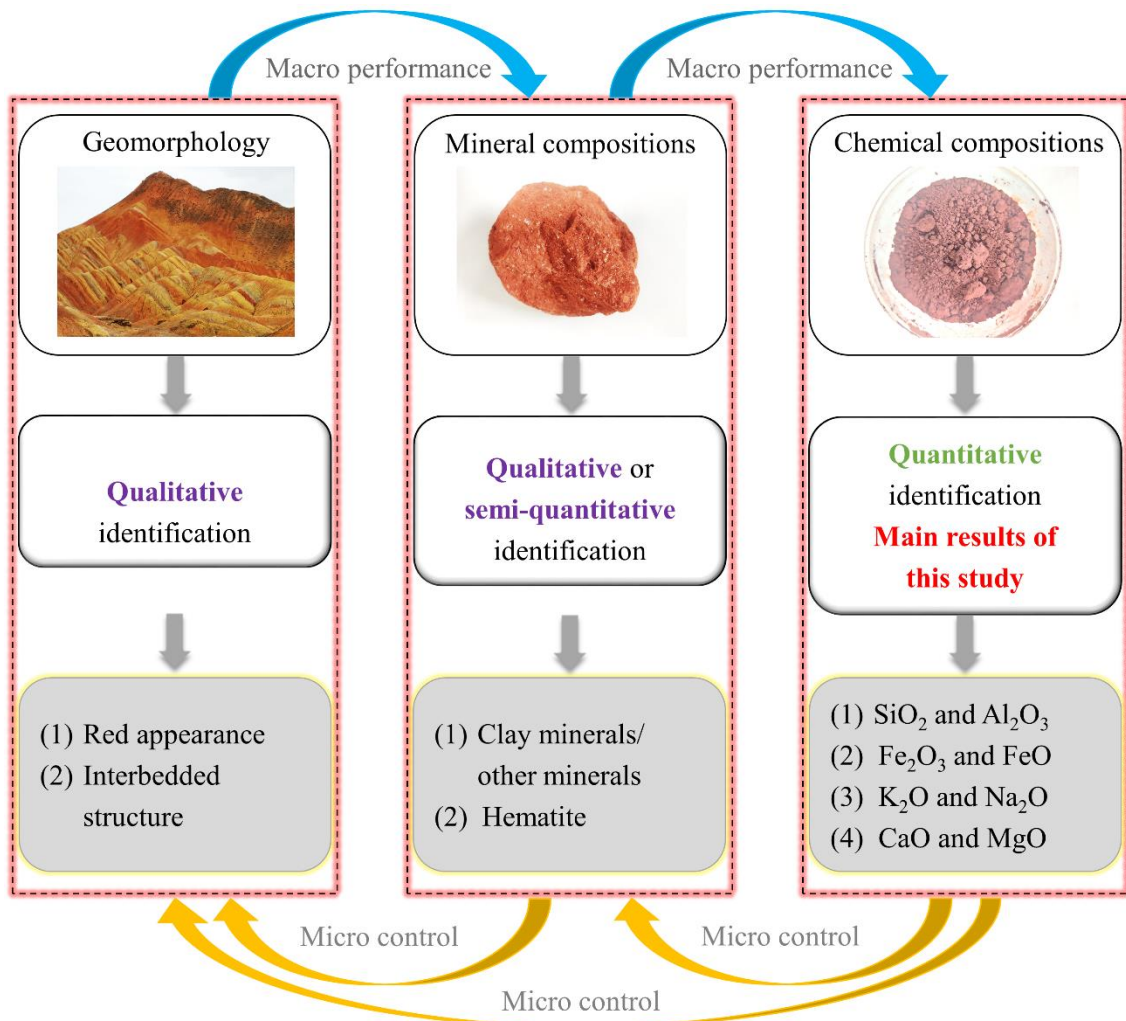
77 Therefore, the purpose of this study to develop a quantitative criterion for quickly and accurately  
78 identifying the red beds. This study first collected the data about the geomorphic characteristics, mineral  
79 content, and chemical composition of red beds and other rocks, then compared these data to obtain the  
80 basic characteristics of red beds, and finally summarized and analyzed the red beds identification  
81 criterion and verified the reliability of this criterion.

82

## 83 **2. Methods**

84 Figure 1 shows the methodology used in this study involving the investigation of geomorphic

85 characteristics, mineral compositions, and chemical compositions (the perspective of chemical  
 86 compositions is the focus of this study). In this study, data on geomorphological features, mineral  
 87 content and chemical composition of the red beds and other rocks were first collected, then these data  
 88 were compared to derive the basic characteristics of the red beds, and finally the red bed identification  
 89 criteria were summarized and analyzed, and the reliability of the criteria was verified.



90

91 **Figure 1.** Methodology for identifying red beds from geomorphic characteristics, mineral  
 92 compositions, and chemical compositions.

93

94 2.1 Data collection

95 The geomorphic characteristics data were collected from the previous studies about landslides,  
 96 debris flows, and collapses on of red beds, igneous rocks (andesite, basalt, diorite, granite),  
 97 metamorphic rocks (gneiss, marble), and other sedimentary rocks (arkose, black-shale, breccia,

98 claystone, dolomite, lignite, limestone, marl, mudstone, siliciclastic, tuff) (e.g., (Zhang et al., 2015; San  
99 et al., 2020; He et al., 2021; Ciftci et al., 2008; Perez-Rey et al., 2019; Anbarasu et al., 2010; Xia et al.,  
100 2019; Gokbulak and Ozcan, 2008; Li et al., 2016; Wang et al., 2022a; Zhang et al., 2017; Underwood  
101 et al., 2016; Kavvadas et al., 2020; Harp et al., 2011; De Montety et al., 2007; Contino et al., 2017; Liu  
102 et al., 2018; Ni et al., 2015; Hale et al., 2021)). The geomorphic characteristics of red beds investigated  
103 in this study involve the evolution process and distribution of red beds on Earth's surface, and the results  
104 were compared with that of other types of rock samples.

105 The mineral compositions of red beds (1,536 groups data) were collected from the previous studies  
106 as shown in Supplementary Table 1 (e.g., (Jian et al., 2009; Liu et al., 2020; Zha et al., 2022; Bai et al.,  
107 2020; Zhang et al., 2021; Zhang et al., 2020; Yao et al., 2016; Li et al., 2023; Marat et al., 2022; Wang  
108 et al., 2017; Chen et al., 2014; Zhang et al., 2016; Li et al., 2015; Li et al., 2013; Wang et al., 2018;  
109 Wang et al., 2014)). These studies used semi quantitative or quantitative methods in XRD technology  
110 to statistically analyze the differences in mineral composition between different red beds (e.g., quartz,  
111 feldspar, mica, hematite, clay minerals, and calcite), as detailed in the aforementioned literatures. This  
112 study mainly focuses on the influence of mineral compositions on geomorphic characteristics,  
113 particularly the layered structure and color of red beds.

114 The chemical compositions of red beds (1536 groups data) with different geological ages and  
115 various lithologies such as conglomerate, sandy conglomerate, sandstone, siltstone, shale and mudstone  
116 were collected from the previous studies as shown in Supplementary Table 2 (e.g., (Uchida et al., 2000;  
117 Xue et al., 2023; Jiang et al., 2022; Yang et al., 2016; Liu et al., 2020; Kong et al., 2018; Zhao et al.,  
118 2005; Gao et al., 2017; Zhang et al., 2008; Liu et al., 2006; Zhu et al., 2003; Liu et al., 2007; Hong et  
119 al., 2009; Wild et al., 2017)). The chemical compositions of igneous rocks, including andesite  
120 (Supplementary Table 3 - 49,203 groups data. Data were downloaded from the GEOROC database  
121 (<https://georoc.mpch-mainz.gwdg.de/georoc/>) on 11 May 2023, using the following parameters: search  
122 = andesite), basalt (Supplementary Table 4 - 80,365 groups data. Data were downloaded from the  
123 GEOROC database on 11 May 2023, using the following parameters: search = basalt), diorite  
124 (Supplementary Table 5 - 4,941 groups data. Data were downloaded from the GEOROC database on  
125 11 May 2023, using the following parameters: search = diorite), and granite (Supplementary Table 6 -

126 17,272 groups data. Data were downloaded from the GEOROC database on 11 May 2023, using the  
127 following parameters: search = granite). The chemical compositions of metamorphic rocks, including  
128 gneiss (Supplementary Table 7 - 24,300 groups data. The data were downloaded from the EarthChem  
129 Portal Database (<http://portal.earthchem.org/>) on 20 April, 2018, using the following parameters:  
130 material = metamorphic and rock name = gneiss) and marble (Supplementary Table 8 - 3,364 groups  
131 data. The data were downloaded from the EarthChem Portal Database on 12 May, 2023, using the  
132 following parameters: material = metamorphic and rock name = marble). The chemical compositions  
133 of other sedimentary rocks, including arkose (Supplementary Table 9 - 682 groups data. The data were  
134 downloaded from the EarthChem Portal Database on 10 May, 2023, using the following parameters:  
135 material = sedimentary and rock name = arkose), black-shale (Supplementary Table 10 - 305 groups  
136 data. The data were downloaded from the EarthChem Portal Database on 10 May, 2023, using the  
137 following parameters: material = sedimentary and rock name = black-shale), breccia (Supplementary  
138 Table 11 - 1,396 groups data. The data were downloaded from the EarthChem Portal Database on 10  
139 May, 2023, using the following parameters: material = sedimentary and rock name = breccia), claystone  
140 (Supplementary Table 12 - 3,790 groups data. The data were downloaded from the EarthChem Portal  
141 Database on 10 May, 2023, using the following parameters: material = sedimentary and rock name =  
142 claystone), dolomite (Supplementary Table 13 - 2,169 groups data. The data were downloaded from the  
143 EarthChem Portal Database on 6 May, 2023, using the following parameters: material = sedimentary  
144 and rock name = dolomite), lignite (Supplementary Table 14 - 3 groups data. The data were downloaded  
145 from the EarthChem Portal Database on 24 April, 2018, using the following parameters: material =  
146 sedimentary and rock name = lignite), limestone (Supplementary Table 15 - 9,104 groups data. The  
147 data were downloaded from the EarthChem Portal Database on 10 May, 2023, using the following  
148 parameters: material = sedimentary and rock name = limestone), marl (Supplementary Table 16 - 142  
149 groups data. The data were downloaded from the EarthChem Portal Database on 10 May, 2023, using  
150 the following parameters: material = sedimentary and rock name = marlstone, marl), mudstone  
151 (Supplementary Table 17 - 6,140 groups data. The data were downloaded from the EarthChem Portal  
152 Database on 10 May, 2023, using the following parameters: material = sedimentary and rock name =  
153 mudstone, mud), siliciclastic (Supplementary Table 18 - 26,938 groups data. The data were downloaded

154 from the EarthChem Portal Database on 10 May, 2023, using the following parameters: material =  
 155 sedimentary and rock name = siliciclastic), tuff (Supplementary Table 19 - 10,295 groups data. The  
 156 data were downloaded from the EarthChem Portal Database on 6 May, 2023, using the following  
 157 parameters: material = sedimentary and rock name = tuff).

158 Studies have found that rock disasters are related to the content of minerals such as quartz, clay  
 159 minerals, hematite, calcite, dolomite, feldspar, etc., and these mineral contents are also closely related  
 160 to the combination of major elements or oxides (Table 1), for example, SiO<sub>2</sub> and Al<sub>2</sub>O<sub>3</sub> (used to study  
 161 the relative content relationship between quartz and clay minerals) (Hong et al., 2009), Fe<sub>2</sub>O<sub>3</sub> and FeO  
 162 (used to study the high content characteristics of hematite) (Hu et al., 2006), CaO and MgO (used to  
 163 study the content relationship of potassium feldspar, calcite, and dolomite) (Han et al., 2023), Na<sub>2</sub>O and  
 164 K<sub>2</sub>O (Qiao et al., 2017). Therefore, this study on the basic chemical composition combination rules and  
 165 quantitative criterion of the red beds only involves the major elements mentioned above, and does not  
 166 involve the analysis of trace elements or other stable isotopes.

167 **Table 1.** Chemical composition (%) of minerals in red beds from database.

Mineral chemical formulas	SiO <sub>2</sub>	Al <sub>2</sub> O <sub>3</sub>	Fe <sub>2</sub> O <sub>3</sub>	FeO	CaO	MgO	Na <sub>2</sub> O	K <sub>2</sub> O	H <sub>2</sub> O	CO <sub>2</sub>
Quartz (SiO <sub>2</sub> )	100.0									
Potassium feldspar (KAlSi <sub>3</sub> O <sub>8</sub> )	64.7	18.4						16.9		
Sodium feldspar (NaAlSi <sub>3</sub> O <sub>8</sub> )	68.8	19.4					11.8			
Calcium feldspar (CaAl <sub>2</sub> Si <sub>2</sub> O <sub>8</sub> )	43.2	36.7			20.1					
White mica (KAl <sub>2</sub> (AlSi <sub>3</sub> O <sub>10</sub> )(OH,F) <sub>2</sub> )	45.2	38.4						11.8	4.1	
Biotite (KMg <sub>3</sub> [Si <sub>3</sub> AlO <sub>10</sub> ](OH,F) <sub>2</sub> )	43.0	12.2				28.8		11.2	2.2	
Phlogopite (K(Mg,Fe) <sub>3</sub> AlSi <sub>3</sub> O <sub>10</sub> (F,OH) <sub>2</sub> )	41.6	11.8		8.3		23.2	0.5	10.9	3.6	
Hematite (Fe <sub>2</sub> O <sub>3</sub> )			100.0							
Calcite (CaCO <sub>3</sub> )					56.0					44.0
Kaolinite (Al <sub>2</sub> Si <sub>2</sub> O <sub>5</sub> (OH) <sub>4</sub> )	46.6	39.5							14.0	
Illite (K <sub>0.75</sub> (Al <sub>1.75</sub> R)[Si <sub>3.5</sub> Al <sub>0.5</sub> O <sub>10</sub> ](OH) <sub>2</sub> )	54.0	17.0		1.9		3.1		7.3	12.0	
Montmorillonite (Na,Ca) <sub>0.33</sub> (Al,Mg) <sub>2</sub> [Si <sub>4</sub> O <sub>10</sub> ](OH) <sub>2</sub> ·nH <sub>2</sub> O	43.8	18.6			1.0		1.1		36.1	
Chlorite (Y <sub>3</sub> [Z <sub>4</sub> O <sub>10</sub> ](OH) <sub>2</sub> ·Y <sub>3</sub> (OH) <sub>6</sub> )	30.3	17.1		15.1		25.4			12.1	

168 Note: Data collected from <http://webmineral.com/> and <https://www.mindat.org/>.

169

170 Using SPSS PRO online data analysis program and principal component analysis method to compare the  
 171 chemical components combination rules of red beds, the identification quantitative criterion was studied at a

172 significance level of  $P < 0.05$ .

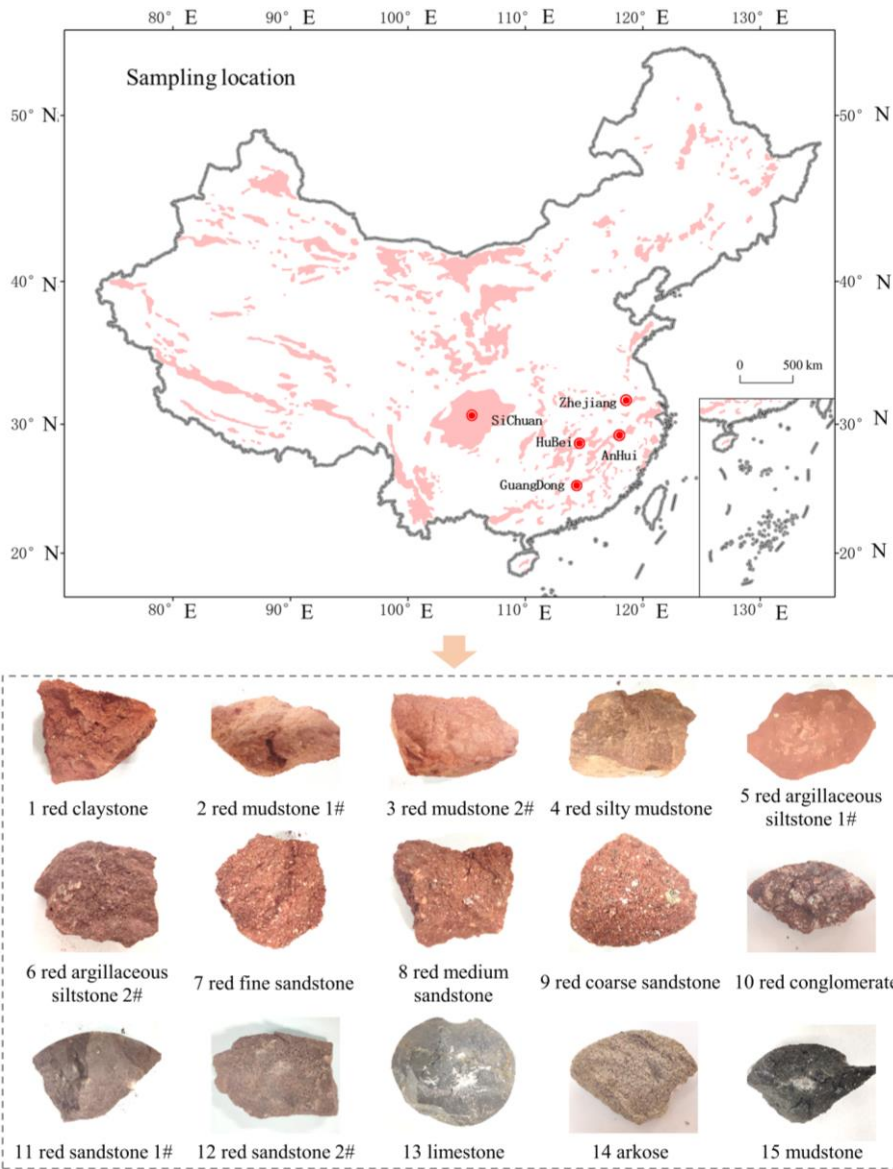
173

## 174 2.2 Criterion verification

175 In order to verify the proposed basic chemical compositions combination rules and quantitative  
176 criterion of red beds, 15 kinds of rocks of known rock types were selected in Guangdong, Sichuan,  
177 Hubei, Zhejiang, and Anhui provinces (Figure 2), including 12 kinds of red beds (red claystone, red  
178 mudstone, red silty mudstone, red argillaceous siltstone, red fine sandstone, red medium sandstone, red  
179 coarse sandstone, red conglomerate, etc.), limestone (1 kind), arkose (1 kind) and mudstone (1 kind).  
180 After on-site sampling, use a hammer to smash the rock block out of the fresh surface. Then, the fresh  
181 surface was analyzed using the YL-P-3LRX Handheld Laser Induced Breakdown Spectroscopy (LIBS,  
182 Figure 3) to check whether these elements conform to the basic chemical compositions combination  
183 rules of red beds proposed by this study. This device can detect elements such as K, Na, Si, Al, Ca, Mg,  
184 Fe, and oxides.

185 The working principle of the LIBS is that a miniature X-ray source provides tube voltage and tube  
186 current, and the light tube emits continuous X-ray spectral lines. The X-rays irradiated on the sample  
187 knock out the inner electrons of the K and L layers of the element atoms, and the holes in the low-  
188 energy layer are filled by high-energy outer electrons (N layer). The high-energy electrons emit excess  
189 energy as X-ray fluorescence ( $K\alpha$ ) with elemental characteristics. Thus, the instrument detects the type  
190 and concentration of elements through the emitted spectral lines. On the instrument analysis interface,  
191 point the detection window towards the rock sample and press the trigger to start and stop the  
192 measurement. After amplification and data collection, the signal is processed to obtain the required test  
193 data.



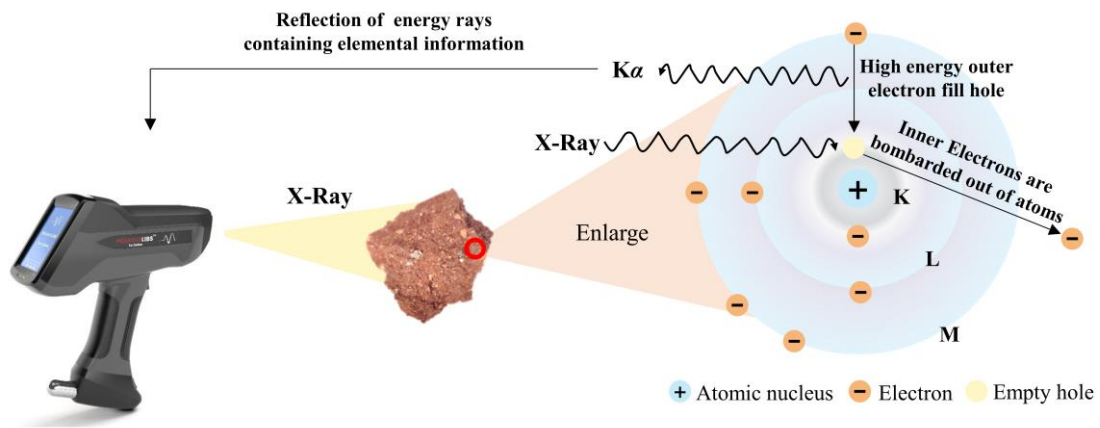


194

195

**Figure 2.** Distribution areas of red beds in China and sampling locations for 15 types of rocks.

196



197

198

**Figure 3.** YL-P-3LRX Handheld Laser Induced Breakdown Spectroscopy and the working principle.

199 **3. Results and discussions**

200 3.1 Geomorphic characteristics of red beds

201 Geomorphic characteristics of the red beds as shown in Figure 4. Red beds are sedimentary rocks  
202 of different geological ages (mainly Mesozoic and Cenozoic) with bedding structure typically  
203 consisting of various lithologies such as conglomerate, sandy conglomerate, sandstone, siltstone, shale  
204 and mudstone that are predominantly red in color due to the presence of ferric oxides (Yan et al., 2019).  
205 Owing to differences in depositional environments and influences of late stage geologic processes, the  
206 color of red beds can be brownish-reddish-yellow, brownish-yellow, purplish-red, brownish-red,  
207 grayish-purple and other reddish tints (Yan et al., 2019; Nance, 2015), making it difficult to accurately  
208 describe using the CIELAB color space and/or Munsell color system. Bedding is a common structural  
209 feature of sedimentary rocks representing the changes in the sedimentary environment. The sandstone  
210 is one of the most common types of red beds, with a distinct reddish appearance. Compared with the  
211 obvious layering and red appearance characteristics of red beds, igneous rocks and metamorphic rocks  
212 do not show the two characteristics of red appearance and bedding at the same time. Basalts are reddish  
213 in appearance but does not have bedding (Cunha et al., 2005). In addition, andesites are mainly light  
214 black and have a columnar structure which is similar to that of basalts (Feizizadeh et al., 2021). Most  
215 of granites are grey or light brown with a significantly different structure compared to red beds (Migon  
216 et al., 2018), while gneisses are generally characterized as a dark and light gneissic structure (Garajeh  
217 et al., 2022). Although the red color appearance and bedding structure can be used as qualitative criteria  
218 for identifying the red beds, the analysis of mineral and chemical compositions is still necessary for  
219 identifying the rocks from quantitative perspective.



220 Red beds Yadan landform

Red beds Danxia landform

221 **Figure 4.** Geomorphic characteristics of the red beds.

222 3.2 Mineral compositions of red beds

223 Table 2 shows the statistical analysis results of mineral compositions of red beds in Supplementary  
 224 Table 1. The common minerals in the red bed are quartz (median value is 40%, the same below), clay  
 225 minerals (35%, including kaolinite, illite, montmorillonite, and chlorite), feldspar (10%, including K-  
 226 feldspar and plagioclase), calcite (10%), mica (7%, including biotite, muscovite and sericite), and  
 227 hematite (3%) according to their content. According to the average value and standard deviation, it can  
 228 be seen that the content range of various minerals has significant dispersion. The ratio of the content of  
 229 clay minerals to other minerals (quartz, feldspar, mica, hematite, and calcite) ranges between 0.11 to  
 230 1.50. The hematite content ranges between 1.5% and 10.0% (percentile=10%~90%), and reddish  
 231 appearance of red beds is due to the abundant hematite content of the rocks. The change in mineral  
 232 compositions of red beds could lead to the change in rock color which is one of the major characteristics  
 233 of red beds. Furthermore, when the red beds encounter water, softening and expansion could happen  
 234 because of the large amount of clay minerals in the rocks, especially the mudstone. The differences in  
 235 mineral compositions of the red beds can also be quantitatively described through their chemical  
 236 composition combination characteristics (Table 1).

237 **Table 2.** The statistical analysis results of mineral compositions of red beds from literature data.

Minerals	Range (per = 0%~100%)	Range (per = 10%~90%)	Median value (per = 50%)	Average value	Standard deviation
Quartz (%)	2.3~94.0	21.0~69.0	40.0	42.6	18.8
Clay minerals (%)	1.0~80.0	7.8~59.0	35.0	34.1	18.6
Feldspar (%)	0.4~71.0	2.3~25.0	10.0	12.6	10.7
Mica (%)	0.1~40.8	3.0~20.0	7.0	9.2	8.2
Hematite (%)	0.4~25.2	1.5~10.0	3.0	5.0	4.4
Calcite (%)	0.7~97.7	3.1~23.5	10.0	12.2	10.0
Clay minerals/ Other minerals	0.01~6.00	0.11~1.50	0.61	0.76	0.66

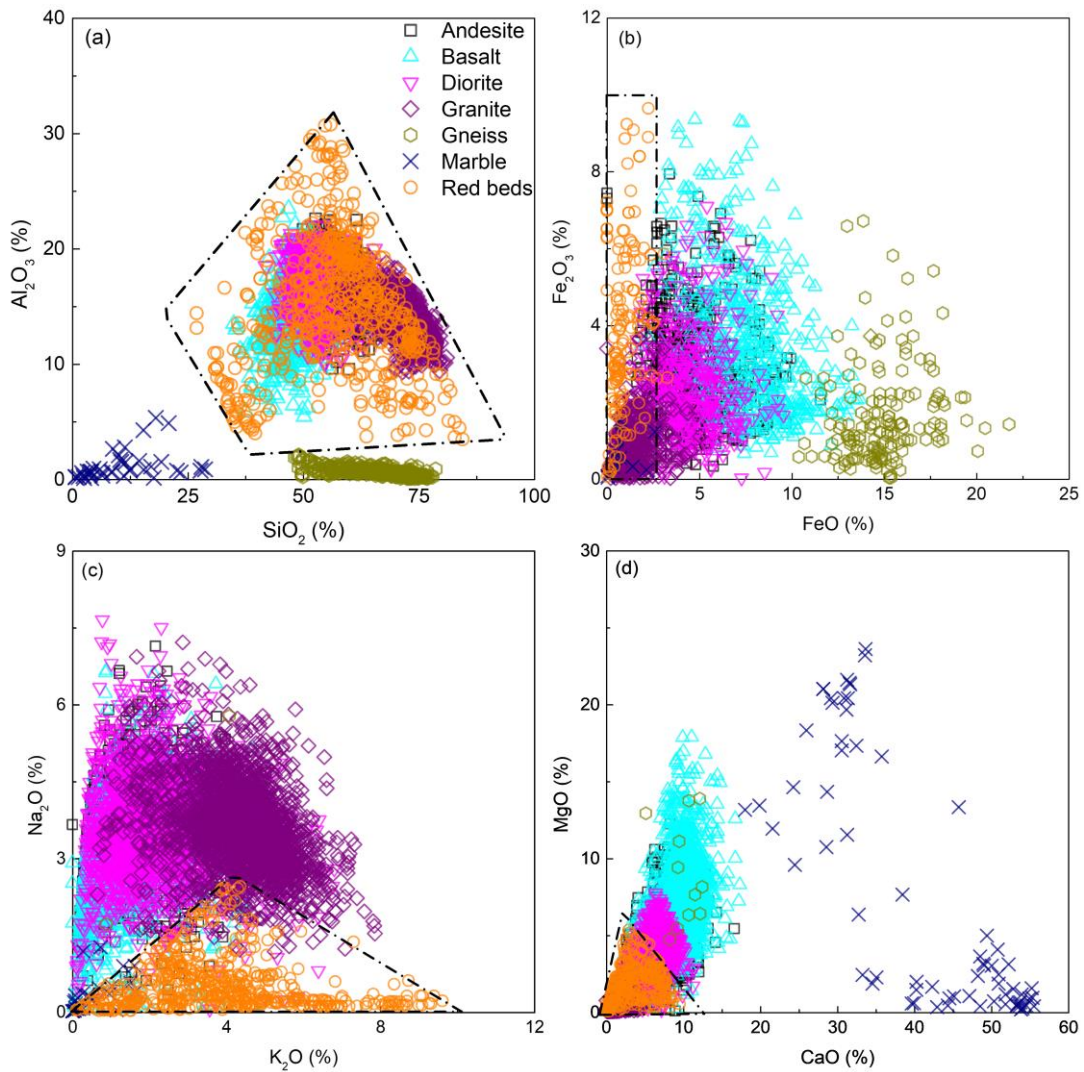
238 Note: per – percentile; Other minerals – quartz, feldspar, mica, hematite, and calcite.

239

240 3.3 Chemical composition characteristics of red beds

241 Figures 5~6 are mainly used to qualitatively analyze the differences in chemical compositions  
 242 between the red beds and other rocks through scatter plots. The area surrounded by black dashed lines  
 243 is the area where the red beds data points are located. To better distinguish various rock data points, the  
 244 distribution areas of various rock data are shown on the right side of the figure, and the corresponding

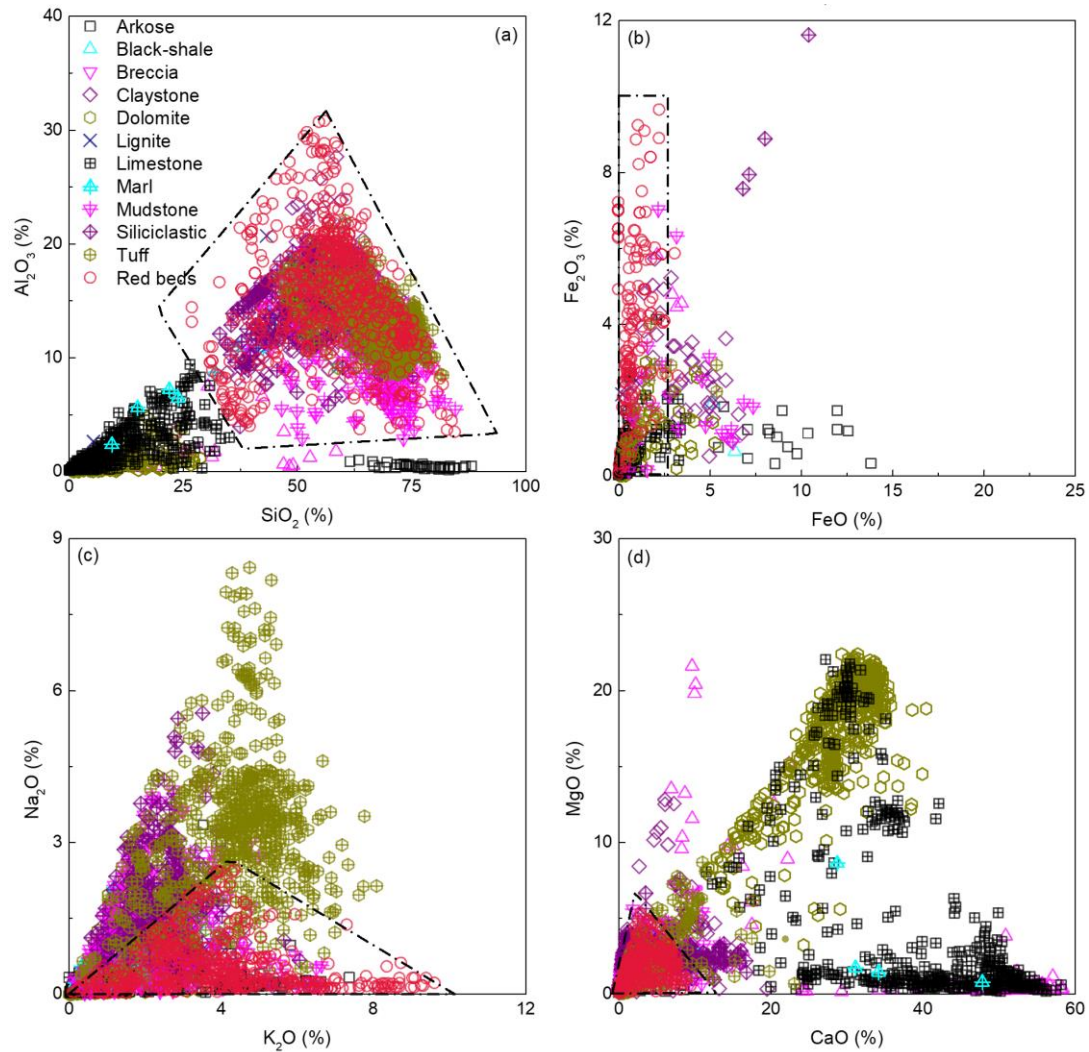
245 colored dashed ellipses are used to indicate the distribution areas in the dataset. Figure 5 shows the  
 246 comparison of  $\text{SiO}_2$  and  $\text{Al}_2\text{O}_3$ ,  $\text{FeO}$  and  $\text{Fe}_2\text{O}_3$ ,  $\text{K}_2\text{O}$  and  $\text{Na}_2\text{O}$ ,  $\text{CaO}$  and  $\text{MgO}$  contents in red beds,  
 247 igneous rocks, and metamorphic rocks, respectively. Figure 6 shows the comparison of  $\text{SiO}_2$  and  $\text{Al}_2\text{O}_3$ ,  
 248  $\text{FeO}$  and  $\text{Fe}_2\text{O}_3$ ,  $\text{K}_2\text{O}$  and  $\text{Na}_2\text{O}$ ,  $\text{CaO}$  and  $\text{MgO}$  contents in red beds and other sedimentary rocks  
 249 respectively.



250

251 **Figure 5.** Comparison of (a)  $\text{SiO}_2$  and  $\text{Al}_2\text{O}_3$ , (b)  $\text{FeO}$  and  $\text{Fe}_2\text{O}_3$ , (c)  $\text{K}_2\text{O}$  and  $\text{Na}_2\text{O}$ , (d)  $\text{CaO}$  and  
 252  $\text{MgO}$  contents in red beds, igneous rock, and metamorphic rocks, respectively. (Note: Icons of the  
 253 same color in the figure have the same meanings)





254

255 **Figure 6.** Comparison of (a) SiO<sub>2</sub> and Al<sub>2</sub>O<sub>3</sub>, (b) FeO and Fe<sub>2</sub>O<sub>3</sub>, (c) K<sub>2</sub>O and Na<sub>2</sub>O, (d) CaO and MgO  
 256 contents in red beds and other sedimentary rocks respectively. (Note: Icons of the same color in the figure  
 257 have the same meanings)

258

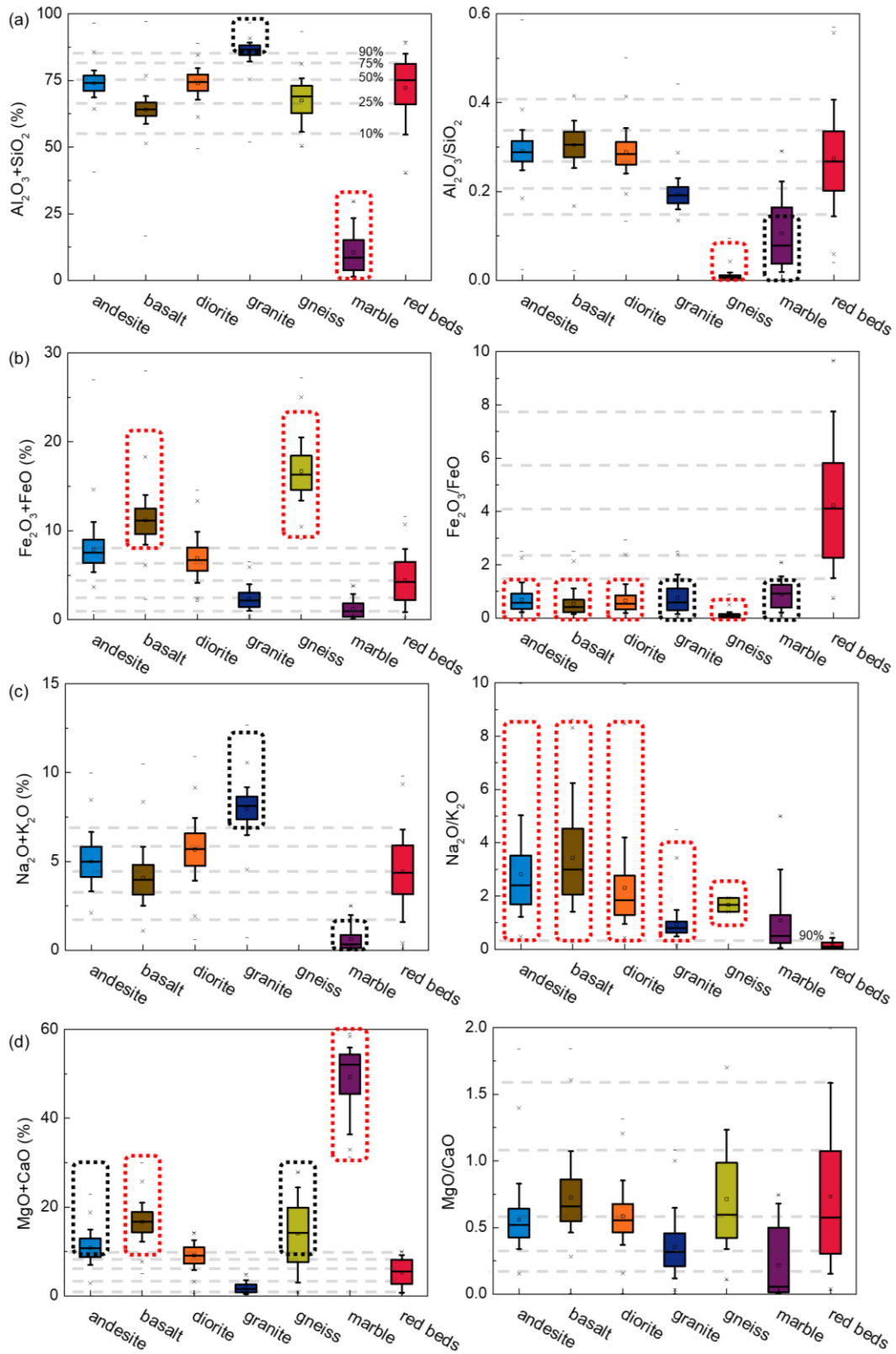
259 The content of SiO<sub>2</sub> in the red beds is about 30%~80%, Al<sub>2</sub>O<sub>3</sub> is about 8%~30%, Fe<sub>2</sub>O<sub>3</sub> is about  
 260 0%~10%, FeO is about 0%~3%, K<sub>2</sub>O is about 0%~10%, Na<sub>2</sub>O is about 0%~2.5%, CaO is about  
 261 0%~10%, and MgO is about 0%~5%. Compared with igneous rocks, metamorphic rocks, and other  
 262 sedimentary rocks, the content of each chemical composition of the red beds has three relationships  
 263 with the content of corresponding chemical composition of other rocks: inclusion relationship (the data  
 264 distribution range of one rock completely covers and is larger than the data range of the other rock),  
 265 intersection relationship (the data distribution range of one rock intersects with the data distribution  
 266 range of another rock), and mutual difference relationship (the data distribution range of one rock does

267 not intersect at all with the data distribution range of another rock). The distribution range of  $\text{SiO}_2$  and  
268  $\text{Al}_2\text{O}_3$  content in the red beds includes the distribution range of  $\text{SiO}_2$  and  $\text{Al}_2\text{O}_3$  content in 9 types of  
269 rocks, namely andesite, basalt, diorite, granite, black shale, claystone, mudstone, siliciclastic, and tuff.  
270 The distribution range of  $\text{SiO}_2$  and  $\text{Al}_2\text{O}_3$  content in the red beds intersects with that in breccia, lignite,  
271 and marl. The distribution range of  $\text{SiO}_2$  and  $\text{Al}_2\text{O}_3$  content in gneiss, marble, arkose, dolomite, and  
272 limestone is different from that in the red beds. The distribution range of  $\text{Fe}_2\text{O}_3$  and FeO content in the  
273 red beds includes the distribution range of  $\text{Fe}_2\text{O}_3$  and FeO content in granite, marble, and lignite. The  
274 distribution range of  $\text{Fe}_2\text{O}_3$  and FeO content in the red beds intersects with that in 8 kinds of rocks,  
275 namely, andesite, basalt, diorite, breccia, claystone, dolomite, limestone, and mudstone. The  
276 distribution range of  $\text{Fe}_2\text{O}_3$  and FeO content in gneiss, arkose, black shale, siliciclastic, and tuff is  
277 different from that in the red beds. The distribution range of  $\text{K}_2\text{O}$  and  $\text{Na}_2\text{O}$  content in the red beds  
278 includes the distribution range of  $\text{K}_2\text{O}$  and  $\text{Na}_2\text{O}$  content in lignite. The distribution range of  $\text{K}_2\text{O}$  and  
279  $\text{Na}_2\text{O}$  content in the red beds intersects with that in 15 kinds of rocks, including andesite, basalt, diorite,  
280 granite, marble, arkose, black shale, breccia, claystone, dolomite, limestone, marl, mudstone,  
281 siliciclastic, and tuff. The distribution range of  $\text{K}_2\text{O}$  and  $\text{Na}_2\text{O}$  content in gneiss is different from that in  
282 the red beds. The distribution range of CaO and MgO content in the red beds includes the distribution  
283 range of CaO and MgO content in granite, black shale, and lignite. The distribution range of CaO and  
284 MgO content in the red beds intersects with that in 13 types of rocks, including andesite, basalt, diorite,  
285 gneiss, arkose, breccia, claystone, dolomite, limestone, marl, mudstone, siliciclastic, and tuff. The  
286 distribution range of CaO and MgO content in marble is different from that in the red beds. Therefore,  
287 from a qualitative perspective, it can be seen that the red beds differ in chemical composition from 8  
288 kinds of rocks, including gneiss, marble, arkose, dolomite, limestone, black-shale, siliciclastic, and tuff,  
289 and also intersects with other rocks to varying degrees. But this is not enough as a criterion to determine  
290 the difference between red beds and other rocks.

291        Figures 7~8 mainly analyze the differences in chemical compositions between red beds and other  
292 rocks through further data statistics and box plots of the scatter plots mentioned above, and propose  
293 quantitative identification criterion for the red beds chemical compositions combination. The red dashed  
294 box in the figure represents rocks that differ from the red beds data, while the black dashed box

295 represents rocks that intersect less than 25% with the red beds data. The data collected in section 2.1  
296 comes from published papers or databases, and its accuracy and robustness have been explained in  
297 relevant literature. In order to ensure the exclusion of outliers in the box plots mentioned above during  
298 the analysis of this study. The horizontal gray dashes corresponding to the red beds box chart represent  
299 10% percentile (the same below), lower quartile (25% percentile), median (50% percentile), upper  
300 quartile (75% percentile), and 90% percentile in the red beds data from bottom to top. Figure 7 shows  
301 the chemical compositions combination comparison of  $\text{SiO}_2+\text{Al}_2\text{O}_3$  (total content, the same below) and  
302  $\text{Al}_2\text{O}_3/\text{SiO}_2$  (content ratio, the same below),  $\text{FeO}+\text{Fe}_2\text{O}_3$  and  $\text{Fe}_2\text{O}_3/\text{FeO}$ ,  $\text{K}_2\text{O}+\text{Na}_2\text{O}$  and  $\text{Na}_2\text{O}/\text{K}_2\text{O}$ ,  
303  $\text{CaO}+\text{MgO}$  and  $\text{MgO}/\text{CaO}$  in red beds, igneous rock, and metamorphic rocks, respectively. Figure 8  
304 respectively shows the chemical compositions combination comparison of  $\text{SiO}_2+\text{Al}_2\text{O}_3$  and  $\text{Al}_2\text{O}_3/\text{SiO}_2$ ,  
305  $\text{FeO}+\text{Fe}_2\text{O}_3$  and  $\text{Fe}_2\text{O}_3/\text{FeO}$ ,  $\text{K}_2\text{O}+\text{Na}_2\text{O}$  and  $\text{Na}_2\text{O}/\text{K}_2\text{O}$ ,  $\text{CaO}+\text{MgO}$  and  $\text{MgO}/\text{CaO}$  in red beds and  
306 other sedimentary rocks.

307 The  $\text{SiO}_2+\text{Al}_2\text{O}_3$  content in the red beds is 54.7%~85.0% (10%~90% percentile, the same below),  
308 the  $\text{Al}_2\text{O}_3/\text{SiO}_2$  ratio is 0.14~0.41, the  $\text{FeO}+\text{Fe}_2\text{O}_3$  content is 0.9%~7.9%, the  $\text{Fe}_2\text{O}_3/\text{FeO}$  ratio is  
309 1.52~7.70, the  $\text{K}_2\text{O}+\text{Na}_2\text{O}$  content is 1.6%~6.8%, the  $\text{Na}_2\text{O}/\text{K}_2\text{O}$  ratio is 0.02~0.43, the  $\text{CaO}+\text{MgO}$   
310 content is 0.8%~9.2%, and the  $\text{MgO}/\text{CaO}$  ratio is 0.16~1.57. By comparing the content of  $\text{SiO}_2+\text{Al}_2\text{O}_3$ ,  
311 the red beds are distinct or have small intersections (less than 25%, the same below) with granite, marble,  
312 dolomite, lignite, limestone, and marl. By comparing the  $\text{Al}_2\text{O}_3/\text{SiO}_2$  ratio, it is found that the red beds  
313 are distinct or have small intersections with gneiss, marble, arkose, and lignite. By comparing the  
314 content of  $\text{FeO}+\text{Fe}_2\text{O}_3$ , it is found that the red beds are distinct or have small intersections with basalt,  
315 gneiss, arkose, and siliciclastic. By comparing the  $\text{Fe}_2\text{O}_3/\text{FeO}$  ratio, it is found that the red beds are  
316 distinct or have small intersections with andesite, basalt, diorite, granite, gneiss, marble, arkose, black  
317 shale, dolomite, mudstone, siliclastic, and tuff. Through the comparison of  $\text{K}_2\text{O}+\text{Na}_2\text{O}$  content, the red  
318 beds are distinct or have small intersections with granite, marble, breccia, dolomite, and limestone. By  
319 comparing the  $\text{Na}_2\text{O}/\text{K}_2\text{O}$  ratio, the red beds are distinct or have small intersections with andesite, basalt,  
320 diorite, gneiss, lignite, siliciclastic, and tuff. Through the comparison of  $\text{CaO}+\text{MgO}$  content, the red  
321 beds are distinct or have small intersections with andesite, basalt, gneiss, marble, breccia, dolomite,  
322 limestone, and marl. By comparing the  $\text{MgO}/\text{CaO}$  ratio, it is difficult to distinguish the red beds from

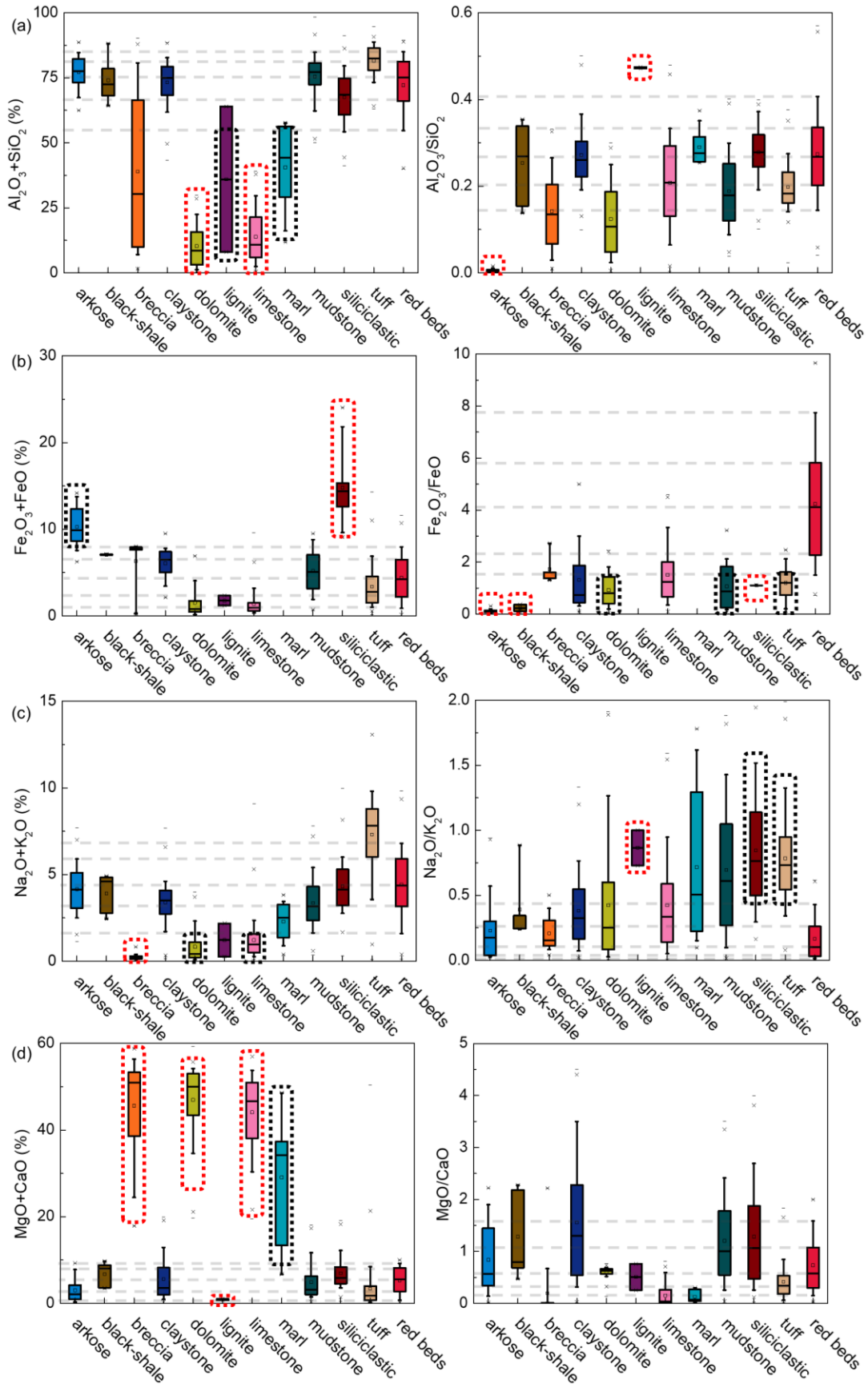


324

325 **Figure 7.** Chemical compositions comparison of (a)  $SiO_2 + Al_2O_3$ ,  $Al_2O_3/SiO_2$ , (b)  $FeO + Fe_2O_3$ ,  $Fe_2O_3/FeO$ ,

326 (c)  $K_2O + Na_2O$ ,  $Na_2O/K_2O$ , (d)  $CaO + MgO$ ,  $MgO/CaO$  in red beds, igneous rock, and metamorphic rocks.





327

328 **Figure 8.** Chemical compositions comparison of (a)  $SiO_2 + Al_2O_3$ ,  $Al_2O_3/SiO_2$ , (b)  $FeO + Fe_2O_3$ ,  $Fe_2O_3/FeO$ ,

329 (c)  $K_2O + Na_2O$ ,  $Na_2O/K_2O$ , (d)  $CaO + MgO$ ,  $MgO/CaO$  in red beds and other sedimentary rocks.

330 In summary, there are differences in chemical compositions between red beds and other rocks.  
 331 Simultaneously meeting the following chemical compositions combinations as a preliminary  
 332 quantitative criterion to distinguish red beds with different geological ages and various lithologies from  
 333 other rocks:  $\text{SiO}_2+\text{Al}_2\text{O}_3 \approx 50.7\%\sim 85.0\%$ ,  $\text{Al}_2\text{O}_3/\text{SiO}_2 \approx 0.14\sim 0.41$ ,  $\text{FeO}+\text{Fe}_2\text{O}_3 \approx 0.9\%\sim 7.9\%$ ,  
 334  $\text{Fe}_2\text{O}_3/\text{FeO} \approx 1.52\sim 7.70$ ,  $\text{K}_2\text{O}+\text{Na}_2\text{O} \approx 1.6\%\sim 6.8\%$ ,  $\text{Na}_2\text{O}/\text{K}_2\text{O} \approx 0.02\sim 0.43$ ,  
 335  $\text{CaO}+\text{MgO} \approx 0.8\%\sim 9.2\%$ , and  $\text{MgO}/\text{CaO} \approx 0.39\sim 1.08$ .

336

### 337 3.4 Principal component analysis and quantitative criterion for red beds identification

338 Based on the preliminary quantitative criterion for identifying the red beds mentioned above, this  
 339 section presents PCA statistical analysis (dimensionality reduction) of the  $\text{SiO}_2+\text{Al}_2\text{O}_3$ ,  $\text{Al}_2\text{O}_3/\text{SiO}_2$ ,  
 340  $\text{FeO}+\text{Fe}_2\text{O}_3$ ,  $\text{Fe}_2\text{O}_3/\text{FeO}$ ,  $\text{K}_2\text{O}+\text{Na}_2\text{O}$ ,  $\text{Na}_2\text{O}/\text{K}_2\text{O}$ ,  $\text{CaO}+\text{MgO}$ , and  $\text{MgO}/\text{CaO}$  of red beds in Figures 7  
 341 and 8. The result is significant with  $P<0.05$  (Table 3), rejecting the null hypothesis. There is correlation  
 342 between the variables, and principal component analysis is effective. It can be seen that the cumulative  
 343 variance interpretation rate of the first five principal components reaches 94.788% (generally greater  
 344 than 90% is sufficient), indicating that using the first five principal components can be well used for  
 345 red beds recognition.

346 **Table 3.** Variance explanation.

Components	Characteristic roots	Variance interpretation rate (%)	Cumulative variance interpretation rate (%)
1	2.700	33.754	33.754
2	2.249	28.112	61.866
3	1.169	14.613	76.479
4	0.882	11.023	87.503
5	0.583	7.285	94.788
6	0.263	3.293	98.081
7	0.131	1.638	99.72
8	0.022	0.280	100.00

347

348 According to the component matrix (Table 4) obtained during the PCA analysis process, the  
 349 calculation equations for 5 principal components  $F1\sim F5$  (Equations 1-5) and the calculation formula  
 350 for the overall principal components  $F$  (Equation 6) can be obtained.

351

352 **Table 4.** Principal component matrix.

Chemical composition combinations	Principal component 1	Principal component 2	Principal component 3	Principal component 4	Principal component 5
SiO <sub>2</sub> +Al <sub>2</sub> O <sub>3</sub>	0.274	-0.281	-0.115	-0.014	-0.009
Al <sub>2</sub> O <sub>3</sub> /SiO <sub>2</sub>	0.085	0.356	0.283	-0.199	-0.352
FeO+Fe <sub>2</sub> O <sub>3</sub>	-0.103	0.334	-0.071	0.449	0.702
Fe <sub>2</sub> O <sub>3</sub> /FeO	0.194	0.038	0.268	0.827	-0.449
K <sub>2</sub> O+Na <sub>2</sub> O	0.213	0.046	0.609	-0.336	0.16
Na <sub>2</sub> O/K <sub>2</sub> O	-0.092	-0.288	0.452	0.179	0.71
CaO+MgO	-0.331	0.05	0.289	-0.153	-0.195
MgO/CaO	0.276	0.196	-0.162	-0.203	0.575

353

$$\begin{aligned}
 354 \quad F1 = & 0.274 \times (\text{SiO}_2 + \text{Al}_2\text{O}_3) + 0.085 \times \left(\frac{\text{Al}_2\text{O}_3}{\text{SiO}_2}\right) - 0.103 \times (\text{FeO} + \text{Fe}_2\text{O}_3) + 0.194 \times \left(\frac{\text{Fe}_2\text{O}_3}{\text{FeO}}\right) \\
 355 \quad & + 0.213 \times (\text{K}_2\text{O} + \text{Na}_2\text{O}) - 0.092 \times \left(\frac{\text{Na}_2\text{O}}{\text{K}_2\text{O}}\right) - 0.331 \times (\text{CaO} + \text{MgO}) + 0.276 \times \left(\frac{\text{MgO}}{\text{CaO}}\right) \quad (1)
 \end{aligned}$$

$$\begin{aligned}
 356 \quad F2 = & -0.281 \times (\text{SiO}_2 + \text{Al}_2\text{O}_3) + 0.356 \times \left(\frac{\text{Al}_2\text{O}_3}{\text{SiO}_2}\right) + 0.334 \times (\text{FeO} + \text{Fe}_2\text{O}_3) + 0.038 \times \left(\frac{\text{Fe}_2\text{O}_3}{\text{FeO}}\right) \\
 357 \quad & + 0.046 \times (\text{K}_2\text{O} + \text{Na}_2\text{O}) - 0.288 \times \left(\frac{\text{Na}_2\text{O}}{\text{K}_2\text{O}}\right) + 0.05 \times (\text{CaO} + \text{MgO}) + 0.196 \times \left(\frac{\text{MgO}}{\text{CaO}}\right) \quad (2)
 \end{aligned}$$

$$\begin{aligned}
 358 \quad F3 = & -0.115 \times (\text{SiO}_2 + \text{Al}_2\text{O}_3) + 0.283 \times \left(\frac{\text{Al}_2\text{O}_3}{\text{SiO}_2}\right) - 0.071 \times (\text{FeO} + \text{Fe}_2\text{O}_3) + 0.268 \times \left(\frac{\text{Fe}_2\text{O}_3}{\text{FeO}}\right) \\
 359 \quad & + 0.609 \times (\text{K}_2\text{O} + \text{Na}_2\text{O}) + 0.452 \times \left(\frac{\text{Na}_2\text{O}}{\text{K}_2\text{O}}\right) + 0.289 \times (\text{CaO} + \text{MgO}) - 0.162 \times \left(\frac{\text{MgO}}{\text{CaO}}\right) \quad (3)
 \end{aligned}$$

$$\begin{aligned}
 360 \quad F4 = & -0.014 \times (\text{SiO}_2 + \text{Al}_2\text{O}_3) - 0.199 \times \left(\frac{\text{Al}_2\text{O}_3}{\text{SiO}_2}\right) + 0.449 \times (\text{FeO} + \text{Fe}_2\text{O}_3) + 0.827 \times \left(\frac{\text{Fe}_2\text{O}_3}{\text{FeO}}\right) \\
 361 \quad & - 0.336 \times (\text{K}_2\text{O} + \text{Na}_2\text{O}) + 0.179 \times \left(\frac{\text{Na}_2\text{O}}{\text{K}_2\text{O}}\right) - 0.153 \times (\text{CaO} + \text{MgO}) - 0.203 \times \left(\frac{\text{MgO}}{\text{CaO}}\right) \quad (4)
 \end{aligned}$$

$$\begin{aligned}
 362 \quad F5 = & -0.009 \times (\text{SiO}_2 + \text{Al}_2\text{O}_3) - 0.352 \times \left(\frac{\text{Al}_2\text{O}_3}{\text{SiO}_2}\right) + 0.702 \times (\text{FeO} + \text{Fe}_2\text{O}_3) - 0.449 \times \left(\frac{\text{Fe}_2\text{O}_3}{\text{FeO}}\right) \\
 363 \quad & + 0.16 \times (\text{K}_2\text{O} + \text{Na}_2\text{O}) + 0.71 \times \left(\frac{\text{Na}_2\text{O}}{\text{K}_2\text{O}}\right) - 0.195 \times (\text{CaO} + \text{MgO}) + 0.575 \times \left(\frac{\text{MgO}}{\text{CaO}}\right) \quad (5)
 \end{aligned}$$

$$364 \quad F = (0.338/0.948) \times F1 + (0.281/0.948) \times F2 + (0.146/0.948) \times F3 + (0.11/0.948) \times F4 + (0.073/0.948) \times F5 \quad (6)$$

365

366 Substituting the relevant data of the red beds in Figures 7 and 8 into Equations 1~6 can calculate  
 367 the quantitative criterion for the red beds:  $F1=-3.36\sim23.55$ ,  $F2=-23.00\sim3.11$ ,  $F3=-10.12\sim4.88$ ,  $F4=-$   
 368  $2.21\sim4.52$ ,  $F5=-0.97\sim7.30$ , and  $F = -0.67\sim1.89$ .

369

### 370 3.5 Red beds identification quantization criterion verification

371 The chemical composition combinations of the 15 selected rocks in this study are shown in Table  
372 5. Study has found that, The rapid detection of  $\text{Fe}^{2+}$  and  $\text{Fe}^{3+}$  is very difficult (Chen et al., 2019) and  
373 exceeds the detection range of handheld laser-induced breakdown spectroscopy in this manuscript and  
374 similar devices. But this factor does not affect the reliability of the quantification criterion for red beds  
375 recognition.  $F1\sim F5$  and  $F$  are considered as 6 evaluation indicators, and there are a total of 72 ( $6 \times 12$ )  
376 evaluation indicators for the 12 types of red beds. Among them, 3 evaluation indicators exceed the  
377 scope of the quantification criterion for red beds identification ( $F4$  of numbered 7, 9, and 11 red beds  
378 with green background in Table 5 is less than the quantification criterion), indicating that the reliability  
379 of detecting these 12 types of rocks belonging to the red beds is as high as 95.8%. And for 3 non red  
380 beds rocks (limestone, arkose, and mudstone), there are a total of 18 evaluation indicators, of which 13  
381 exceed the scope of the quantification criterion for red beds identification (indicated by blue  
382 background), indicating a high reliability of 72.2% in detecting these three types of rocks that do not  
383 belong to the red beds. Therefore, this study proposes a quantitative criterion for red beds recognition  
384 with high reliability. In the future, if there are new devices that can quickly detect  $\text{Fe}^{2+}$  and  $\text{Fe}^{3+}$ , the  
385 recognition efficiency of the red beds recognition quantification criterion in this study will be higher.  
386

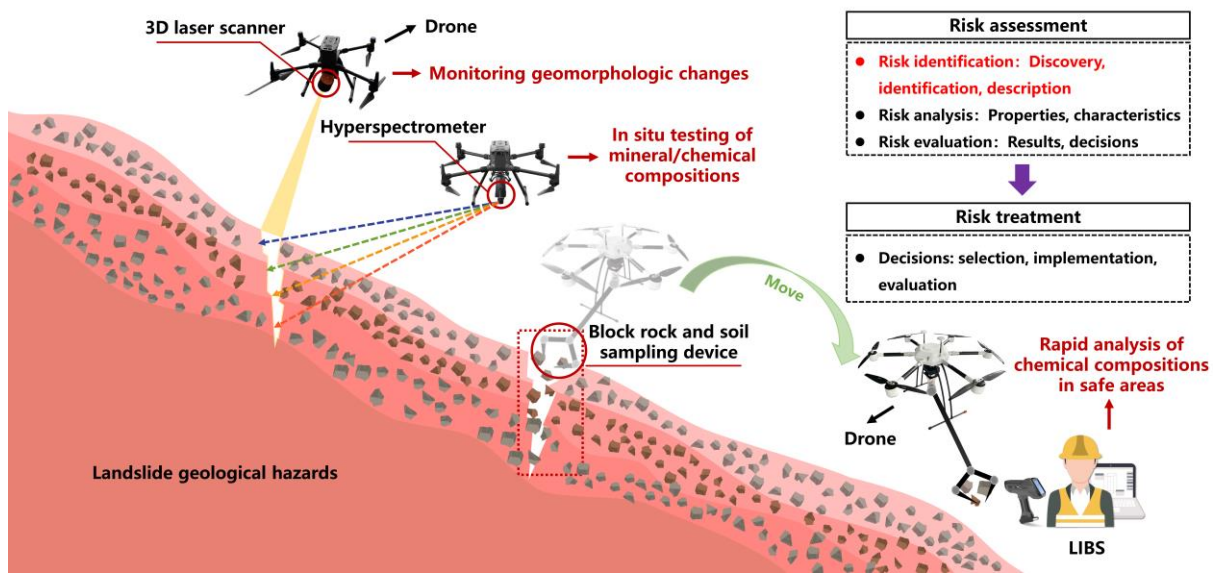
387 **Table 5.** Chemical composition combinations of 15 kinds of rocks.

No.	SiO <sub>2</sub> (%)	Al <sub>2</sub> O <sub>3</sub> (%)	TFe <sub>3</sub> O <sub>4</sub> (%)	Na <sub>2</sub> O (%)	K <sub>2</sub> O (%)	MgO (%)	CaO (%)	F1	F2	F3	F4	F5	F	Rock types
1	63.67	18.56	7.41	0.56	5.60	4.2	-	21.71	-20.06	-4.89	-0.58	4.60	1.33	Red beds
2	65.43	18.29	6.18	0.07	3.56	6.47	-	20.96	-20.88	-5.90	-0.66	2.82	0.52	
3	69.68	10.95	7.12	0.88	2.43	3.64	5.30	19.27	-19.59	-5.08	-0.52	3.66	0.50	
4	62.6	17.89	6.98	1.47	5.24	5.82	-	20.84	-19.67	-3.78	-1.14	4.21	1.21	
5	69.92	13.59	6.93	0.22	5.19	4.15	-	21.96	-20.64	-5.53	-0.54	4.13	1.12	
6	71.16	13.55	3.33	0.39	2.83	3.27	5.47	20.83	-21.96	-5.47	-2.24	0.76	-0.13	
7	68.63	15.74	1.33	1.61	4.86	2.83	5.00	21.91	-22.48	-3.47	-4.06	0.16	0.16	
8	64.53	15.67	6.75	0.30	5.35	3.6	3.80	20.31	-19.40	-4.18	-1.35	3.98	1.00	
9	69.11	15.63	4.21	0.68	5.98	4.38	-	22.76	-21.83	-4.61	-2.23	2.41	0.86	
10	66.58	11.66	7.41	1.53	4.05	8.77	-	18.94	-18.86	-3.37	-0.95	3.89	0.83	
11	73.04	11.46	1.6	1.39	3.34	2.97	6.20	21.07	-22.50	-4.15	-3.51	-0.15	-0.22	
12	70.47	12.35	6.33	1.26	5.47	1.49	2.63	22.26	-20.54	-4.62	-1.32	4.40	1.32	
13	30.36	2.35	0.15	0.33	0.28	0.70	65.84	-13.05	-6.10	16.38	-10.58	-12.25	-6.11	Limestone
14	75.27	12.73	2.22	2.47	4.59	2.67	0.06	36.73	-14.90	-12.11	-12.00	27.27	7.52	Arkose
15	78.33	18.86	1.00	0.25	1.04	0.53	-	26.62	-26.87	-10.13	-1.43	0.02	-0.20	Mudstone

388 **Note:** TFe<sub>3</sub>O<sub>4</sub> represents the content of Fe<sub>2</sub>O<sub>3</sub> and FeO. "-" represents that no content was detected. Ignoring "Fe<sub>2</sub>O<sub>3</sub>/FeO" and "MgO/CaO" without values when calculating F1-F5  
389 and F.

390 3.6 Research results application methods

391 Figure 9 shows the application methods of the research results. According to the methods for  
392 emergency management of landslide geological disasters (Fu et al., 2021), landslide risk assessment  
393 (including risk identification, risk analysis, and risk assessment) and risk management (developing and  
394 selecting treatment plans, as well as planning, implementing, and evaluating treatment methods) need  
395 to be carried out before the landslide occurs. In the field of engineering geology, risk identification is  
396 the most important prerequisite for landslide emergency response. Red beds is the slippery layer that  
397 needs to be identified in risk identification.



398  
399 **Figure 9.** Research results used for risk identification.

400

401 At present, the commonly used risk identification method is to use drones to carry image capture  
402 devices for three-dimensional reconstruction of slope images, determine the volume of landslide  
403 accumulation, and determine the shape changes of the slope (Chen et al., 2020; Fu et al., 2021), which  
404 can be also used for mountain rescue (Wankmuller et al., 2021). Based on the drone technology,  
405 combined with the Optech Polaris LR 3D laser scanner and the HY-9070 hyperspectral analyzer of Sun  
406 Yat-sen University, the landslide shape change and remote monitoring of mineral and chemical  
407 compositions can be realized to identify whether it is a red beds landslide. It can also use a drone  
408 equipped with a block rock and soil sampling device to collect representative blocks of rock and soil  
409 within cracks to a safe area, and then use the YL-P-3LRX Handheld Laser Induced Breakdown

410 Spectroscopy for rapid analysis. Therefore, the research results can be used for rapid identification of  
411 red beds, achieving risk assessment and rapid response of geological disasters such as landslides.

412

#### 413 **4. Conclusions**

414 (1) In response to the rapid identification of red beds in geological disaster emergency response, a  
415 rapid quantitative identification criterion based on the basic chemical compositions combination rules  
416 of red beds has been established, taking into account the correlation between red beds geomorphic  
417 characteristics, mineral compositions, and chemical compositions. It solves the current problem of  
418 fuzzy identification of the red beds.

419 (2) The results indicate that the red beds in the geomorphic characteristics have obvious interlayer  
420 characteristics and its appearance is red. In mineral composition, the ratio of clay minerals to other  
421 minerals of red beds ranges from 0.11 to 1.50, and the content of hematite of red beds ranges from 1.5%  
422 to 10.0%. The following chemical composition combinations can be used as red beds preliminary  
423 quantification criterion:  $\text{SiO}_2+\text{Al}_2\text{O}_3 \approx 50.7\% \sim 85.0\%$ ,  $\text{Al}_2\text{O}_3/\text{SiO}_2 \approx 0.14 \sim 0.41$ ,  
424  $\text{FeO}+\text{Fe}_2\text{O}_3 \approx 0.9\% \sim 7.9\%$ ,  $\text{Fe}_2\text{O}_3/\text{FeO} \approx 1.52 \sim 7.70$ ,  $\text{K}_2\text{O}+\text{Na}_2\text{O} \approx 1.6\% \sim 6.8\%$ ,  
425  $\text{Na}_2\text{O}/\text{K}_2\text{O} \approx 0.02 \sim 0.43$ ,  $\text{CaO}+\text{MgO} \approx 0.8\% \sim 9.2\%$ . And the principal component features can serve  
426 as a rapid quantitative criterion for distinguishing red beds:  $F_1 = -3.36 \sim 23.55$ ,  $F_2 = -23.00 \sim 3.11$ ,  $F_3 =$   
427  $10.12 \sim 4.88$ ,  $F_4 = -2.21 \sim 4.52$ ,  $F_5 = -0.97 \sim 7.30$ , and  $F = -0.67 \sim 1.89$ . The reliability of the quantitative  
428 criterion was verified by collecting 15 kinds of rocks and analyzing their chemical composition  
429 combinations.

430 (3) The combination of research results with existing landslide geological hazard risk identification  
431 techniques can effectively carry out rapid response to geological disasters, which is very important for  
432 emergency response to geological disasters. Moreover, the research results can also be applied to the  
433 quantitative identification of red beds in other fields such as resources, ecology, environment, energy,  
434 materials, etc.

435

#### 436 **Declarations**

437 **Availability of data and materials**

438 The data that support the findings of this study are available in supplementary materials.

439 **Competing interests**

440 The authors declare no conflict of interest. The funders had no role in the design of the study; in  
441 the collection, analyses, or interpretation of data; in the writing of the manuscript, or in the decision to  
442 publish the results.

443 **Funding**

444 The research is supported by the National Natural Science Foundation of China (NSFC) (Grant  
445 Numbers: 42293354, 42277131, 42293351, 42293355 and 42293350).

446 **Authors' contributions**

447 Conceptualization, C.Z. and Z.L.; methodology, G.C. and Z.L.; software, G.C. and L.K.; validation,  
448 G.C., L.K., and Z.L.; formal analysis, C.Z. and Z.L.; investigation, G.C., J.L., and L.Y.; resources, G.C.  
449 and L.K.; data curation, G.C., J.L., L.Y. and L.K.; writing—original draft preparation, G.C. and L.K.;  
450 writing—review and editing, G.C., Z.L., and L.Z.; visualization, L.Y.; supervision, Z.L. and L.Z.;  
451 project administration, C.Z.; funding acquisition, C.Z. All authors have read and agreed to the published  
452 version of the manuscript.

453 **Acknowledgments**

454 The authors would like to thank the anonymous reviewers for their very constructive and helpful  
455 comments.

456 **Supplementary Materials**

457 Supplementary Table 1: Mineral compositions of the red beds.

458 Supplementary Table 2: Chemical compositions of the red beds.

459 Supplementary Table 3: Chemical compositions of the andesite.

460 Supplementary Table 4: Chemical compositions of the basalt.

461 Supplementary Table 5: Chemical compositions of the diorite.

462 Supplementary Table 6: Chemical compositions of the granite.

463 Supplementary Table 7: Chemical compositions of the gneiss.

464 Supplementary Table 8: Chemical compositions of the marble.



465 Supplementary Table 9: Chemical compositions of the arkose.  
466 Supplementary Table 10: Chemical compositions of the black-shale.  
467 Supplementary Table 11: Chemical compositions of the breccia.  
468 Supplementary Table 12: Chemical compositions of the claystone.  
469 Supplementary Table 13: Chemical compositions of the dolomite.  
470 Supplementary Table 14: Chemical compositions of the lignite.  
471 Supplementary Table 15: Chemical compositions of the limestone.  
472 Supplementary Table 16: Chemical compositions of the marl.  
473 Supplementary Table 17: Chemical compositions of the mudstone.  
474 Supplementary Table 18: Chemical compositions of the siliciclastic.  
475 Supplementary Table 19: Chemical compositions of the tuff.

476

## 477 **References**

- 478 Anbarasu, K., Sengupta, A., Gupta, S., and Sharma, S. P.: Mechanism of activation of the Lanta Khola landslide  
479 in Sikkim Himalayas, *Landslides*, 7, 135-147, 10.1007/s10346-009-0193-0, 2010.
- 480 Bai, Y., Shan, R., Ju, Y., Wu, Y., Tong, X., Han, T., and Dou, H.: Experimental study on the strength, deformation  
481 and crack evolution behaviour of red sandstone samples containing two ice-filled fissures under triaxial  
482 compression, *Cold Regions Science and Technology*, 174, 10.1016/j.coldregions.2020.103061, 2020.
- 483 Bankole, O. M., Albani, A. E., Meunier, A., Rouxel, O. J., Oisgauthier-Lafaye, F., and Bekker, A.: Origin of Red  
484 Beds in the Paleoproterozoic Franceville Basin, Gabon, and Implications for Sandstone-Hosted Uranium  
485 Mineralization, *Am J Sci*, 316, 839-872, 10.2475/09.2016.02, 2016.
- 486 Chen, J., Dai, F., Xu, L., Chen, S., Wang, P., Long, W., and Shen, N.: Properties and microstructure of a natural  
487 slip zone in loose deposits of red beds, southwestern China, *Eng Geol*, 183, 53-64,  
488 10.1016/j.enggeo.2014.10.004, 2014.
- 489 Chen, L. F., Tian, X. K., Xia, D. S., Nie, Y. L., Lu, L. Q., Yang, C., and Zhou, Z. X.: Novel Colorimetric Method  
490 for Simultaneous Detection and Identification of Multimetal Ions in Water: Sensitivity, Selectivity, and  
491 Recognition Mechanism, *Acs Omega*, 4, 5915-5922, 10.1021/acsomega.9b00312, 2019.
- 492 Chen, S. J., Xiang, C. C., Kang, Q., Zhong, W., Zhou, Y. L., and Liu, K.: Accurate landslide detection leveraging  
493 UAV-based aerial remote sensing, *Iet Commun*, 14, 2434-2441, 10.1049/iet-com.2019.1115, 2020.

494 Chen, Z. Y., Männik, P., Fan, J. X., Wang, C. Y., Chen, Q., Sun, Z. Y., Chen, D. Y., and Li, C.: Age of the Silurian  
495 Lower Red Beds in South China: Stratigraphical Evidence from the Sanbaiti Section, *J Earth Sci-China*, 32,  
496 524-533, [10.1007/s12583-020-1350-6](https://doi.org/10.1007/s12583-020-1350-6), 2021.

497 Ciftci, E., Hogan, J. P., Kolayli, H., and Cadirli, E.: Natrolite, an unusual rock - Occurrence and petrographic  
498 and geochemical characteristics (eastern Turkey), *Clay Clay Miner*, 56, 207-221,  
499 [10.1346/Ccmn.2008.0560206](https://doi.org/10.1346/Ccmn.2008.0560206), 2008.

500 Contino, A., Bova, P., Esposito, G., Giuffre, I., and Monteleone, S.: Historical analysis of rainfall-triggered  
501 rockfalls: the case study of the disaster of the ancient hydrothermal Sclafani Spa (Madonie Mts, northern-  
502 central Sicily, Italy) in 1851, *Nat Hazard Earth Sys*, 17, 2229-2243, [10.5194/nhess-17-2229-2017](https://doi.org/10.5194/nhess-17-2229-2017), 2017.

503 Cui, G., Zhou, C., Liu, Z., Xia, C., and Zhang, L.: The synthesis of soft rocks based on physical and mechanical  
504 properties of red mudstone, *International Journal of Rock Mechanics and Mining Sciences*, 151, 105037,  
505 <https://doi.org/10.1016/j.ijrmms.2022.105037>, 2022.

506 Cunha, P., Marques, J., Curi, N., Pereira, G. T., and Lepsch, I. F.: Geomorphic surfaces and latosol (oxisol)  
507 characteristics on a sandstone/basalt sequence from the Jaboticabal region, Sao Paulo State, Brazil, *Rev Bras*  
508 *Cienc Solo*, 29, 81-90, [Doi 10.1590/S0100-06832005000100009](https://doi.org/10.1590/S0100-06832005000100009), 2005.

509 de Montety, V., Marc, V., Emblanch, C., Malet, J. P., Bertrand, C., Maquaire, O., and Bogaard, T. A.: Identifying  
510 the origin of groundwater and flow processes in complex landslides affecting black marls: insights from a  
511 hydrochemical survey, *Earth Surf Proc Land*, 32, 32-48, [10.1002/esp.1370](https://doi.org/10.1002/esp.1370), 2007.

512 Feizizadeh, B., Garajeh, M. K., Blaschke, T., and Lakes, T.: An object based image analysis applied for volcanic  
513 and glacial landforms mapping in Sahand Mountain, Iran, *Catena*, 198, ARTN 105073  
514 [10.1016/j.catena.2020.105073](https://doi.org/10.1016/j.catena.2020.105073), 2021.

515 Fu, L., Zhu, J., Li, W.-l., You, J.-g., and Hua, Z.-y.: Fast estimation method of volumes of landslide deposit by  
516 the 3D reconstruction of smartphone images, *Landslides*, 18, 3269-3278, [10.1007/s10346-021-01702-9](https://doi.org/10.1007/s10346-021-01702-9),  
517 2021.

518 Gao, F., Wu, X., and Deng, R.: The distribution of red beds and analysis on engineering characteristics of  
519 mudstone in Guangxi, *Journal of Geological Hazards and Environment Preservation*, 28, 48-52, 2017.

520 Garajeh, M. K., Feizizadeh, B., Blaschke, T., and Lakes, T.: Detecting and mapping karst landforms using object-  
521 based image analysis: Case study: Takht-Soleiman and Parava Mountains, Iran, *The Egyptian Journal of*  
522 *Remote Sensing and Space Science*, 25, 473-489, <https://doi.org/10.1016/j.ejrs.2022.03.009>, 2022.

523 Gokbulak, F. and Ozcan, M.: Hydro-physical properties of soils developed from different parent materials,  
524 Geoderma, 145, 376-380, 10.1016/j.geoderma.2008.04.006, 2008.

525 Hale, S., Ries, X., Jaeggi, D., and Blum, P.: Mechanical and hydraulic properties of the excavation damaged zone  
526 (EDZ) in the Opalinus Clay of the Mont Terri rock laboratory, Switzerland, Solid Earth, 12, 1581-1600,  
527 10.5194/se-12-1581-2021, 2021.

528 Han, P. H., Zhang, C., Wang, X. J., and Wang, L.: Study of mechanical characteristics and damage mechanism  
529 of sandstone under long-term immersion, Eng Geol, 315, ARTN 107020  
530 10.1016/j.enggeo.2023.107020, 2023.

531 Harp, E. L., Dart, R. L., and Reichenbach, P.: Rock fall simulation at Timpanogos Cave National Monument,  
532 American Fork Canyon, Utah, USA, Landslides, 8, 373-379, 10.1007/s10346-010-0251-7, 2011.

533 He, J., Niu, F., Luo, F., Jiang, H., He, P., and Ju, X.: Mechanical properties and modified binary-medium  
534 constitutive model for red-bed soft rock subjected to freeze-thaw cycles, Cold Reg Sci Technol, 209,  
535 10.1016/j.coldregions.2023.103803, 2023.

536 He, K., Ma, G. T., and Hu, X. W.: Formation mechanisms and evolution model of the tectonic-related ancient  
537 giant basalt landslide in Yanyuan County, China, Nat Hazards, 106, 2575-2597, 10.1007/s11069-021-04555-  
538 6, 2021.

539 Hong, H., Li, Z., and Xiao, P.: Clay Mineralogy Along the Laterite Profile in Hubei, South China: Mineral  
540 Evolution and Evidence for Eolian Origin, Clay Clay Miner, 57, 602-615, 10.1346/Ccmn.2009.0570508,  
541 2009.

542 Hu, X., Wang, C., Li, X., and Luba, J.: Upper Cretaceous oceanic red beds in southern Tibet: Lithofacies,  
543 environments and colour origin, Sci China Ser D, 49, 785-795, 10.1007/s11430-006-0785-7, 2006.

544 Jian, W. X., Wang, Z. J., and Yin, K. L.: Mechanism of the Anlesi landslide in the Three Gorges Reservoir, China,  
545 Eng Geol, 108, 86-95, 10.1016/j.enggeo.2009.06.017, 2009.

546 Jiang, H., Xia, Y., Li, J., Liu, S., Zhang, M., and Wang, Y.: Controlling the Iron Migration Mechanism for the  
547 Cretaceous Sediment Color Variations in Sichuan Basin, China, Acs Omega, 7, 480-495,  
548 10.1021/acsomega.1c04893, 2022.

549 Kavvas, M., Roumpos, C., and Schilizzi, P.: Stability of Deep Excavation Slopes in Continuous Surface Lignite  
550 Mining Systems, Geotechnical and Geological Engineering, 38, 791-812, 10.1007/s10706-019-01066-x,  
551 2020.

552 Kirsch, M., Lorenz, S., Zimmermann, R., Tusa, L., Mockel, R., Hodl, P., Booyesen, R., Khodadadzadeh, M., and  
553 Gloaguen, R.: Integration of Terrestrial and Drone-Borne Hyperspectral and Photogrammetric Sensing  
554 Methods for Exploration Mapping and Mining Monitoring, *Remote Sens-Basel*, 10, 10.3390/rs10091366,  
555 2018.

556 Kong, L. W., Zeng, Z. X., Bai, W., and Wang, M.: Engineering geological properties of weathered swelling  
557 mudstones and their effects on the landslides occurrence in the Yanji section of the Jilin-Hunchun high-speed  
558 railway, *B Eng Geol Environ*, 77, 1491-1503, 10.1007/s10064-017-1096-2, 2018.

559 Li, A., Deng, H., Zhang, H., Liu, H., and Jiang, M.: The shear-creep behavior of the weak interlayer mudstone in  
560 a red-bed soft rock in acidic environments and its modeling with an improved Burgers model, *Mech Time-  
561 Depend Mat*, 27, 1-18, 10.1007/s11043-021-09523-y, 2023.

562 Li, J., Xu, Q., Hu, Z., Liu, H., Zhang, Q., Lu, Y., and Wang, S.: Experimental research on softening of undisturbed  
563 saturated slip soil in eastern of Sichuan province red bed, *Chinese Journal of Rock Mechanics and  
564 Engineering*, 34, 4333-4342, 2015.

565 Li, S., Chen, J., and Yi, G.: Experimental study on the relationship between micro-characteristics and compressive  
566 strength of the red bed rock, *Geotechnical Investigation and Surveying*, 41, 1-5, 2013.

567 Li, X. N., Zhu, B. L., and Wu, X. Y.: Swelling characteristics of soils derived from black shales heightened by  
568 cations in Northern Chongqing, China, *J Mt Sci-Engl*, 13, 1107-1119, 10.1007/s11629-015-3576-9, 2016.

569 Liu, C., He, C., and He, M.: Engineering geology study on failure of red beds slopes along railway in the west of  
570 Hunan Province, *The Chinese Journal of Geological Hazard and Control*, 18, 58-62, 2007.

571 Liu, J., Wei, J. H., Hu, H., Wu, J. M., Sun, S. R., and Kanungo, D. P.: Research on the engineering geological  
572 conditions and stability evaluation of the B2 talus slide at the Jin'an Bridge hydropower station, China, *B  
573 Eng Geol Environ*, 77, 105-125, 10.1007/s10064-017-1005-8, 2018.

574 Liu, J., Xu, Q., Wang, S., Siva Subramanian, S., Wang, L., and Qi, X.: Formation and chemo-mechanical  
575 characteristics of weak clay interlayers between alternative mudstone and sandstone sequence of gently  
576 inclined landslides in Nanjiang, SW China, *B Eng Geol Environ*, 79, 4701-4715, 10.1007/s10064-020-  
577 01859-y, 2020.

578 Liu, X., Zhao, M., Su, Y., and Long, Y.: Grey Correlation Analysis of Slake Durability of Red Bed Weak Rock,  
579 *Journal of Hunan University (Natural Sciences)*, 33, 16-20, 2006.

580 Marat, A. R., Tamas, T., Samsudean, C., and Gheorghiu, R.: Physico-Mechanical and Mineralogical  
581 Investigations of Red Bed Slopes (Cluj-Napoca, Romania), *B Eng Geol Environ*, 81, 10.1007/s10064-021-  
582 02542-6, 2022.

583 Migon, P., Woo, K. S., and Kasprzak, M.: Landform Recognition in Granite Mountains in East Asia (Seoraksan,  
584 Republic of Korea, and Huangshan and Sanqingshan, China) - a Contribution of Geomorphology to the  
585 Unesco World Heritage, *Quaest Geogr*, 37, 103-114, 10.2478/quageo-2018-0008, 2018.

586 Moonjun, R., Shrestha, D. P., Jetten, V. G., and van Ruitenbeek, F. J. A.: Application of airborne gamma-ray  
587 imagery to assist soil survey: A case study from Thailand, *Geoderma*, 289, 196-212,  
588 10.1016/j.geoderma.2016.10.035, 2017.

589 Nance, H. S.: Interfingering of evaporites and red beds: an example from the queen/grayburg formation, Texas,  
590 *Sediment Geol*, 56, 357-381, 2015.

591 Ni, L. T., Zhong, J. H., Shao, Z. F., Li, Y., Mao, C., and Liu, S. X.: Characteristics, Genesis, and Sedimentary  
592 Environment of Duplex-Like Structures in the Jurassic Sediments of Western Qaidam Basin, China, *J Earth  
593 Sci-China*, 26, 677-689, 10.1007/s12583-015-0578-2, 2015.

594 Perez-Rey, I., Riquelme, A., Gonzalez-deSantos, L. M., Estevez-Ventosa, X., Tomas, R., and Alejano, L. R.: A  
595 multi-approach rockfall hazard assessment on a weathered granite natural rock slope, *Landslides*, 16, 2005-  
596 2015, 10.1007/s10346-019-01208-5, 2019.

597 Perri, F., Critelli, S., Martín-Algarra, A., Martín-Martín, M., Perrone, V., Mongelli, G., and Zattin, M.: Triassic  
598 redbeds in the Malaguide Complex (Betic Cordillera - Spain): Petrography, geochemistry and geodynamic  
599 implications, *Earth-Sci. Rev.*, 117, 1-28, 10.1016/j.earscirev.2012.11.002, 2013.

600 Qiao, L. P., Wang, Z. C., and Huang, A. D.: Alteration of Mesoscopic Properties and Mechanical Behavior of  
601 Sandstone Due to Hydro-Physical and Hydro-Chemical Effects, *Rock Mechanics and Rock Engineering*, 50,  
602 255-267, 10.1007/s00603-016-1111-0, 2017.

603 Rainoldi, A. L., Franchini, M., Beaufort, D., Mozley, P., Giusiano, A., Nora, C., Patrier, P., Impiccini, A., and  
604 Pons, J.: Mineral reactions associated with hydrocarbon paleomigration in the Huincul High, Neuquen Basin,  
605 Argentina, *Geol Soc Am Bull*, 127, 1711-1729, 10.1130/B31201.1, 2015.

606 San, N. E., Topal, T., and Akin, M. K.: Rockfall Hazard Assessment Around Ankara Citadel (Turkey) Using  
607 Rockfall Analyses and Hazard Rating System, *Geotechnical and Geological Engineering*, 38, 3831-3851,  
608 10.1007/s10706-020-01261-1, 2020.

609 Triantafyllou, A., Mattielli, N., Clerbois, S., Da Silva, A. C., Kaskes, P., Claeys, P., Devleeschouwer, X., and  
610 Brkojewitsch, G.: Optimizing multiple non-invasive techniques (PXRF, pMS, IA) to characterize coarse-  
611 grained igneous rocks used as building stones, *J Archaeol Sci*, 129, 10.1016/j.jas.2021.105376, 2021.

612 Uchida, E., Ogawa, Y., Maeda, N., and Nakagawa, T.: Deterioration of stone materials in the Angkor monuments,  
613 Cambodia, *Eng Geol*, 55, 101-112, Doi 10.1016/S0013-7952(99)00110-6, 2000.

614 Underwood, S. J., Schultz, M. D., Berti, M., Gregoretti, C., Simoni, A., Mote, T. L., and Saylor, A. M.:  
615 Atmospheric circulation patterns, cloud-to-ground lightning, and locally intense convective rainfall  
616 associated with debris flow initiation in the Dolomite Alps of northeastern Italy, *Nat Hazard Earth Sys*, 16,  
617 509-528, 10.5194/nhess-16-509-2016, 2016.

618 Wang, D., Li, X.-b., Peng, K., Ma, C., Zhang, Z., and Liu, X.: Geotechnical characterization of red shale and its  
619 indication for ground control in deep underground mining, *J Cent South Univ*, 25, 2979-2991,  
620 10.1007/s11771-018-3968-4, 2018.

621 Wang, F. W., Chen, Y., Peng, X. L., Zhu, G. L., Yan, K. M., and Ye, Z. H.: The fault-controlled Chengtian  
622 landslide triggered by rainfall on 20 May 2021 in Songyang County, Zhejiang Province, China, *Landslides*,  
623 19, 1751-1765, 10.1007/s10346-022-01891-x, 2022a.

624 Wang, L., Wang, L., Zhang, W., Meng, X., Liu, S., and Zhu, C.: Time series prediction of reservoir bank landslide  
625 failure probability considering the spatial variability of soil properties, *J Rock Mech Geotech*,  
626 <https://doi.org/10.1016/j.jrmge.2023.11.040>, 2024.

627 Wang, M., Qi, Y. A., Li, D., Dai, M. Y., and Chang, Y. G.: Ichnofabrics and Their Environmental Interpretation  
628 from the Fluvial Deposits of the Middle Triassic Youfangzhuang Formation in Western Henan, Central China,  
629 *J Earth Sci-China*, 25, 648-661, 10.1007/s12583-014-0454-2, 2014.

630 Wang, Y., Liu, J., Yan, S., Yu, L., and Yin, K.: Estimation of probability distribution of shear strength of slip  
631 zone soils in Middle Jurassic red beds in Wanzhou of China, *Landslides*, 14, 2165-2174, 10.1007/s10346-  
632 017-0890-z, 2017.

633 Wang, Y., Tang, H., Huang, J., Wen, T., Ma, J., and Zhang, J.: A comparative study of different machine learning  
634 methods for reservoir landslide displacement prediction, *Eng Geol*, 298, 106544,  
635 <https://doi.org/10.1016/j.enggeo.2022.106544>, 2022b.

636 Wankmuller, C., Kunovjanek, M., and Mayrgundter, S.: Drones in emergency response-evidence from cross-  
637 border, multi-disciplinary usability tests, *Int J Disast Risk Re*, 65, 10.1016/j.ijdr.2021.102567, 2021.

638 Wild, K. M., Walter, P., and Amann, F.: The response of Opalinus Clay when exposed to cyclic relative humidity  
639 variations, *Solid Earth*, 8, 351-360, 10.5194/se-8-351-2017, 2017.

640 Wu, L. Z., Zhang, L. M., Zhou, Y., Xu, Q., Yu, B., Liu, G. G., and Bai, L. Y.: Theoretical analysis and model test  
641 for rainfall-induced shallow landslides in the red-bed area of Sichuan, *Bulletin of Engineering Geology and  
642 the Environment*, 77, 1343-1353, 10.1007/s10064-017-1126-0, 2018.

643 Xia, K. Z., Chen, C. X., Zheng, Y., Zhang, H. N., Liu, X. M., Deng, Y. Y., and Yang, K. Y.: Engineering geology  
644 and ground collapse mechanism in the Chengchao Iron-ore Mine in China, *Eng Geol*, 249, 129-147,  
645 10.1016/j.enggeo.2018.12.028, 2019.

646 Xue, Y., Wang, Q., Ma, L., Yu, Y., and Zhang, R.: Mechanisms and controlling factors of heave in summer for  
647 high-speed railway cutting: A case study of Northwest China, *Construction and Building Materials*, 365,  
648 10.1016/j.conbuildmat.2022.130061, 2023.

649 Yan, L. B., Peng, H., Zhang, S. Y., Zhang, R. X., Kasanin-Grubin, M., Lin, K. R., and Tu, X. J.: The Spatial  
650 Patterns of Red Beds and Danxia Landforms: Implication for the formation factors-China, *Sci Rep-Uk*, 9,  
651 10.1038/s41598-018-37238-7, 2019.

652 Yang, Y., Zhou, J., Xu, F., and Xing, H.: An Experimental Study on the Water-Induced Strength Reduction in  
653 Zigong Argillaceous Siltstone with Different Degree of Weathering, *Adv Mater Sci Eng*,  
654 10.1155/2016/4956986, 2016.

655 Yao, H., Jia, S., Gan, W., Zhang, Z., and Lu, K.: Properties of Crushed Red-Bed Soft Rock Mixtures Used in  
656 Subgrade, *Adv Mater Sci Eng*, 2016, 10.1155/2016/9624974, 2016.

657 Zha, F., Huang, K., Kang, B., Sun, X., Su, J., Li, Y., and Lu, Z.: Deterioration Characteristic and Constitutive  
658 Model of Red-Bed Argillaceous Siltstone Subjected to Drying-Wetting Cycles, *Lithosphere-Uk*, 2022,  
659 8786210, 10.2113/2022/8786210, 2022.

660 Zhang, M., Yin, Y., and Huang, B.: Mechanisms of rainfall-induced landslides in gently inclined red beds in the  
661 eastern Sichuan Basin, SW China, *Landslides*, 12, 973-983, 10.1007/s10346-015-0611-4, 2015.

662 Zhang, S., Xu, Q., and Hu, Z. M.: Effects of rainwater softening on red mudstone of deep-seated landslide,  
663 Southwest China, *Eng Geol*, 204, 1-13, 10.1016/j.enggeo.2016.01.013, 2016.

664 Zhang, W., Lin, S., Wang, L., Wang, L., Jiang, X., and Wang, S.: A novel creep contact model for rock and its  
665 implement in discrete element simulation, *Comput Geotech*, 167, 106054,  
666 <https://doi.org/10.1016/j.compgeo.2023.106054>, 2024.

667 Zhang, Y., Li, F., and Chen, J.: Analysis of the interaction between mudstone and water, *Journal of Engineering*  
668 *Geology*, 16, 22-26, 2008.

669 Zhang, Z., Gao, W., Zeng, C., Tang, X., and Wu, J.: Evolution of the disintegration breakage of red-bed soft rock  
670 using a logistic regression model, *Transp Geotech*, 24, 10.1016/j.trgeo.2020.100382, 2020.

671 Zhang, Z. H., Chen, X. C., Yao, H. Y., Huang, X., and Chen, L. W.: Experimental Investigation on Tensile  
672 Strength of Jurassic Red-Bed Sandstone under the Conditions of Water Pressures and Wet-Dry Cycles, *Ksce*  
673 *J Civ Eng*, 25, 2713-2724, 10.1007/s12205-021-1404-z, 2021.

674 Zhang, Z. L., Wang, T., Wu, S. R., Tang, H. M., and Liang, C. Y.: The role of seismic triggering in a deep-seated  
675 mudstone landslide, China: Historical reconstruction and mechanism analysis, *Eng Geol*, 226, 122-135,  
676 10.1016/j.enggeo.2017.06.001, 2017.

677 Zhao, M., Liu, X., and Su, Y.: Experimental studies on engineering properties of red bed material containing  
678 slaking rock, *Chinese Journal of Geotechnical Engineering*, 27, 667-671, 2005.

679 Zhou, C., Hu, Y., Xiao, T., Ou, Q., and Wang, L.: Analytical model for reinforcement effect and load transfer of  
680 pre-stressed anchor cable with bore deviation, *Construction and Building Materials*, 379, 131219,  
681 <https://doi.org/10.1016/j.conbuildmat.2023.131219>, 2023a.

682 Zhou, C., Yu, L., Huang, Z., Liu, Z., and Zhang, L.: Analysis of microstructure and spatially dependent  
683 permeability of soft soil during consolidation deformation, *Soils Found*, 61, 708-733,  
684 <https://doi.org/10.1016/j.sandf.2021.02.004>, 2021.

685 Zhou, C., Liu, Z., Xue, Y., Li, Y., Fan, X., Chen, W., and Sun, P.: Some thoughts on basic research of red beds  
686 disaste, *Journal of Engineering Geology*, 31, 689-705, 10.13544/j.cnki.jeg.2022-0842, 2023b.

687 Zhu, B., Hu, H., and Chen, Q.: Preliminary study on the characteristics and hazards of M - shaped roadcut slope  
688 in red beds, *Journal of Engineering Geology*, 11, 411-415, 2003.

689